SELECTIVE MANIPULATION OF ICT AND PeT PROCESSES IN STYRYL-BODIPY DERIVATIVES: APPLICATIONS IN MOLECULAR LOGIC AND FLUORESCENCE SENSING OF METAL IONS

A THESIS
SUBMITTED TO THE INSTITUTE OF ENGINEERING AND SCIENCES
OF BILKENT UNIVERSITY
IN PARTIAL FULFILLMENT OF THE REQUIREMENTS
FOR THE DEGREE OF
MASTER OF SCIENCE

By
SENCER SELÇUK
July 2010

I certify that I have read this thesis and that in my opinion it is fully adequate, in scope and in quality, as a thesis of the degree of Master of Science.

…….

Prof. Dr. Engin U. Akkaya (Principal Advisor)

I certify that I have read this thesis and that in my opinion it is fully adequate, in scope and in quality, as a thesis of the degree of Master of Science.

…….

Prof. Dr. Ömer Dağ

I certify that I have read this thesis and that in my opinion it is fully adequate, in scope and in quality, as a thesis of the degree of Master of Science.

…….

Asst. Prof. Dr. Dönüş Tuncel

I certify that I have read this thesis and that in my opinion it is fully adequate, in scope and in quality, as a thesis of the degree of Master of Science.

…….

Asst. Prof. Dr. Neslihan Şaki

I certify that I have read this thesis and that in my opinion it is fully adequate, in scope and in quality, as a thesis of the degree of Master of Science.

…….

Asst. Prof. Dr. M. Fatih Danışman

Approved for the Institute of Engineering and Science:

…….

Prof. Dr. Levent Onural

Director of the Institute of Engineering and Science

ABSTRACT

SELECTIVE MANIPULATION OF ICT AND PeT PROCESSES IN STYRYL-BODIPY DERIVATIVES: APPLICATIONS IN MOLECULAR LOGIC AND FLUORESCENCE SENSING OF METAL IONS

Sencer Selçuk
M.Sc. in Chemistry
Supervisor: Prof. Dr. Engin U. Akkaya
July, 2010

Recent developments in the Bodipy chemistry, provided new opportunities for modification of this chromophore which, in turn, using appropriate metal-ligand pairs, allowed the control and manipulation of PeT and ICT mechanisms. Exploiting these mechanisms, we demonstrated that photophysical properties of Bodipy can be shaped as desired using metal cation modulators to obtain absorbance signals in accordance with a digital half-adder circuit. In addition, another Bodipy derivative with a simple and rational design, shown to have emission signals equivalent to **AND** operation in Boolean logic. A molecular three-input **AND** gate was also synthesized taking the advantage of differential binding affinities of metal cations for different ligands. Our work proves that, with careful design, photophysical properties of a single chromophore can be modified as desired. Hence molecular logic gates, and even molecules performing more complex logic operations can be obtained using metal cations as non-annihilating logic inputs.

ÖZET

STIRIL-BODIPY TÜREVLERINDE PeT VE ICT MEKANIZMALARININ SEÇICI KONTROLÜ: MOLEKÜLER MANTIK DEVRELERI VE METAL KATYONLARI IÇIN FLORESANS SENSÖRLERDE UYGULAMALAR

Sencer Selçuk
Kimya Bölümü, Yüksek Lisans
Tez Yöneticisi: Prof. Dr. Engin U. Akkaya
Temmuz, 2010

Bodipy kimyasındaki son yıllardaki gelişmeler, bu kromoforun çok çeşitli şekillerde modifikasyonuna olanak sağladı. Bu olanak, uygun ligand-metal çiftleri kullanılarak Bodipy üzerinde ışıkla indüklenen elektron transferi (PeT) ve molekül içi yük transferi (ICT) mekanizmalarinin istenildiği şekilde kontrol ve manipüle edilebilmesini de sağladı. Biz de bu çalışmamızda Bodipy'nin fotofiziksel özelliklerini metal katyonları ile kontrol ederek emisyon sinyallerinin sayısal mantıktaki yarım toplayıcı işlemine benzer bir şekilde elde edilebileceğini gösterdik. Bunun yanında basit ve rasyonel bir tasarımla elde ettiğimiz, yine Bodipy türevi bir molekülün emisyon sinyallerinin Boole mantığındaki **VE** işlemine eşdeğer olduğunu gözlemledik. Ayrıca metallerin farklı ligandlara ilgilerinin farklı olmasını kullanarak üç girdili bir **VE** kapısı da elde ettik. Çalışmamız dikkatli bir dizaynla tek bir kromofor üzerinde fotofiziksel özelliklerin istenildiği şekilde modifiye edilebileceğini, böylece birbirini kimyasal olarak yok etmeyen farklı metal katyonlarının girdi olarak kullanıldığı moleküler mantık kapılarının ve daha kompleks moleküler mantık işlemcilerinin yapılabileceğini gösteriyor.

ACKNOWLEDGEMENT

I am heartily thankful to my supervisor Engin U. Akkaya whose encouragement and support made this work possible. I also owe gratitude to him for his great patience and understanding during the course this research .

I want to thank our group members Özgür Altan Bozdemir, Gökhan Barın, Ruslan Guliyev, Hande Boyacı, Tuğrul Nalbantoğlu, Yusuf Çakmak, Safacan Kölemen, Onur Büyükçakır, Sündüs Erbaş, Tuğba Özdemir, Fazlı Sözmen, Bilal Kılıç, Merve Türkşanlı and rest of the SCL (Supramolecular Chemistry Laboratory) members some of whom participated also in this research,.

I would like to thank to TÜBİTAK (The Scientific and Technological Research Council of Turkey) for financial support.

TABLE OF CONTENTS

LIST OF FIGURES

LIST OF TABLES

LIST OF ABBREVIATIONS

ASTM	**:**	American Society for Testing and Materials
Bodipy	**:**	Boradiazaindacene
DDQ	**:**	Dichlorodicyanoquinone
DFT	**:**	Density Functional Theory
DMF	**:**	Dimethylformamide
EnT	**:**	Energy Transfer
HOMO	**:**	Highest Occupied Molecular Orbital
ICT	**:**	Internal Charge Transfer
ITC	**:**	Isothermal Titration Calorimetry
IYTE	**:**	İzmir Yüksek Teknoloji Enstitüsü
LUMO	**:**	Lowest Unoccupied Molecular Orbital
MALDI:	**:**	Matrix-Assisted Laser Desorption/Ionization
MS	**:**	Mass Spectroscopy
NMR	**:**	Nuclear Magnetic Resonance
PeT	**:**	Photoinduced Electron Transfer
pMOS	**:**	Positive-Channel Metal Oxide Semiconductor
TFA	**:**	Trifluoroacetic Acid
THF	**:**	Tetrahydrofuran
TLC	**:**	Thin Layer Chromotography
TOF	**:**	Time of Flight

CHAPTER 1

INTRODUCTION

1.1 Supramolecular Chemistry: *Quo Vadis?*

Considering the Pedersen's paper[1] as the signal flare, not even half a century passed since the beginning of supramolecular chemistry. Today, however, one of the pioneering names of the field, J. Fraser Stoddart argues[2] the end of supramolecular chemistry –at least with its classical understanding. His point can be summarized simply by saying: Lehn's "chemistry of intermolecular bonds"[3] once claimed much but achieved less. He notes we still have no molecular device at hand that commercialized on a grand scale and offers a way out of this jam: to forsake simple systems for complex ones and to work with surfaces and interfaces rather than working with solution or solid phases[2] –which he brands *"another biology"*.

It is the dignity of science that there is no final authority. One –even a masters student- can disagree with this position of a pioneering professor and examine its validity. *Another biology* may even be possible. And if it is, it will probably have striking applications, even will create its own fields of application. But the crucial question is that, will it be possible to make *two different biologies* to talk each other? Why should we forsake the possibility of supramolecular chemistry that talks the same language as our bodies –ours and the whole biosphere's- from the beginning?

The only viable answer could have been *"because it is not possible!"* Recently, however, promising works[4,5] demonstrated the existence of such a possibility. These researches, on molecular logic gates, a relatively young subfield of supramolecular chemistry, seem to imply emergence of a much natural supramolecular chemistry than Professor Stoddard anticipated.

1.2 Logic Gates: Workhorses of Modern IT[6]

"…and of this I am fully assured, that no *general* method for the solution of questions in the theory of probabilities can be established which does not explicitly recognize, not only the special numerical bases of the science, but also those universal laws of thought which are the basis of all reasoning, and which, whatever they may be as to their essence, are at least

mathematical as to their form." says[7] George Boole in a communication paper he sent to Philosophical Magazine in 1853. These universal laws of thought he mentioned, today called Boolean logic, are the mathematical tools that structured modern information technology.

Table 1. All possible two-input Boolean Logic operations.

INPUTS		OUTPUTS							
A	B	FALSE	AND	A NOT B	A	B NOT A	B	XOR	OR
0	0	0	0	0	0	0	0	0	0
0	1	0	0	0	0	1	1	1	1
1	0	0	0	1	1	0	0	1	1
1	1	0	1	0	1	0	1	0	1
INPUTS		OUTPUTS							
A	B	NOR	XNOR	NOT B	A → B	NOT A	B → A	NAND	TRUE
0	0	1	1	1	1	1	1	1	1
0	1	0	0	0	0	1	1	1	1
1	0	0	0	1	1	0	0	1	1
1	1	0	1	0	1	0	1	0	1

Boolean logic constructs the operational basis of all digital computers since the first examples built during World War II, immutably. What is changed during the course of time is mainly size, cost and energy consumption of the elements that actually performs the logic operations –logic gates. An important landmark in this change of logic gate architecture is production of first silicon-based semiconductor[8] at Texas Instruments in 1954. Modern logic gates are implemented electronically using silicon-based semiconductor technology for almost sixty years, which achieved thirty thousand-fold miniaturization in terms of weight[9], six thousand times less energy consumption[10] and even enhancements in processor speed.

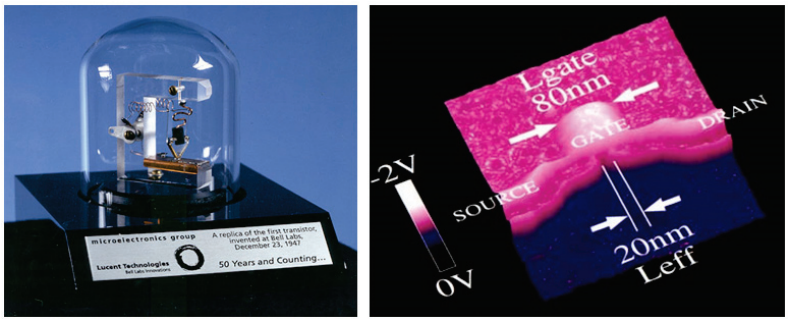

Figure 1. Replica of first silicon-based transistor[11] compared with a state-of-art pMOS transistor[12].

Miniaturization, still, is a consistently pressing demand of IT market and it followed a regular trend until recently as Intel cofounder Gordon E. Moore predicted[13] in 1965 "for at least ten years" (Figure 2). Around 2020, however, current technology is expected to hit a dead-end in terms of miniaturization due to quantum tunneling effect[14] and chip manufacturers started to plan post-transistor era of logic gates. Away from commercialization yet, *molecular logic gates* is being pronounced as a possible solution, stronger day after day.

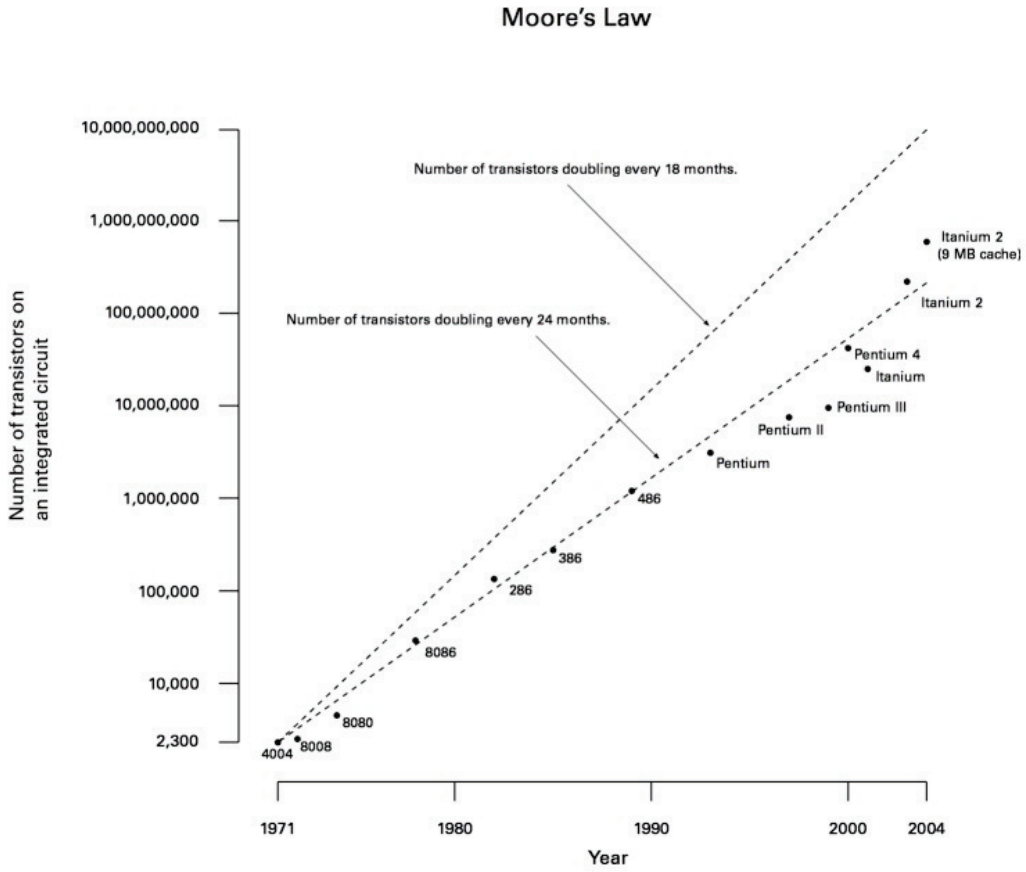

Figure 2. CPU transistor counts 1971-2004 and Moore's Law[15]

1.2.1 Molecular Logic Gates: Computing at the Bottom

One of the topics Feynman debuted in his famous speech "*There is plenty of room at the bottom"* was miniaturizing the computer[16]: "I don't know how to do this on a small scale in a practical way, but I do know that computing machines are very large." We still do not know a practical way, but since the seminal paper[17] of P. A. de Silva has been published in Nature in 1993, we have some ideas. One of the various **AND** gate architectures presented in this paper is shown in Figure 3 along with the truth table, that responds to Na^+ and H^+ cations in terms of fluorescence signal.

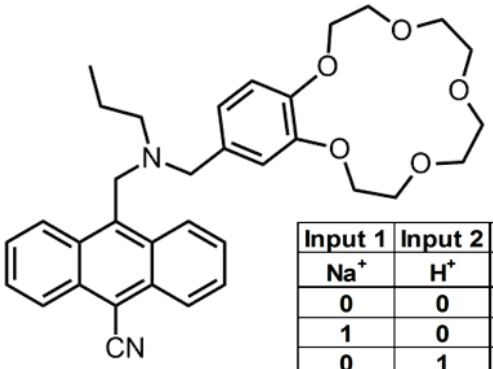

Input 1	Input 2	Output	
Na^+	H^+	Q.Y.	F.enhancement
0	0	0.011	1.0
1	0	0.020	1.8
0	1	0.013	1.2
1	1	0.068	6.2

Figure 3. First two-input molecular logic device designed by de Silva along with truth table adapted fluorescence measurements

Such systems with optical output signals are, not exclusively but widely preferred in molecular logic gates studies. Fluorescent logic gates are the main concern of this thesis and in order to explain the working principles, fluorescence and mechanisms of its modulation will be covered briefly before further development.

1.2.2 Basics of Fluorescence

Light emission from any substance is called luminescence and it is formally divided into two categories as fluorescence and phosphorescence. This distinction is based on the nature of light-emitting electronic excited state. If the excited state is a singlet one, since the excited electron is paired to an electron in the ground state, relaxation occurs rapidly. The term fluorescence is coined[18] for this process by G. G. Stokes in 1852. Typical lifetime for an excited fluorophore is about 10 ns[19]. For triplet excited states, however, since transitions to the ground state are spin-forbidden, emission rates are much slower compared to fluorescence. These transitions are called phosphorescence.

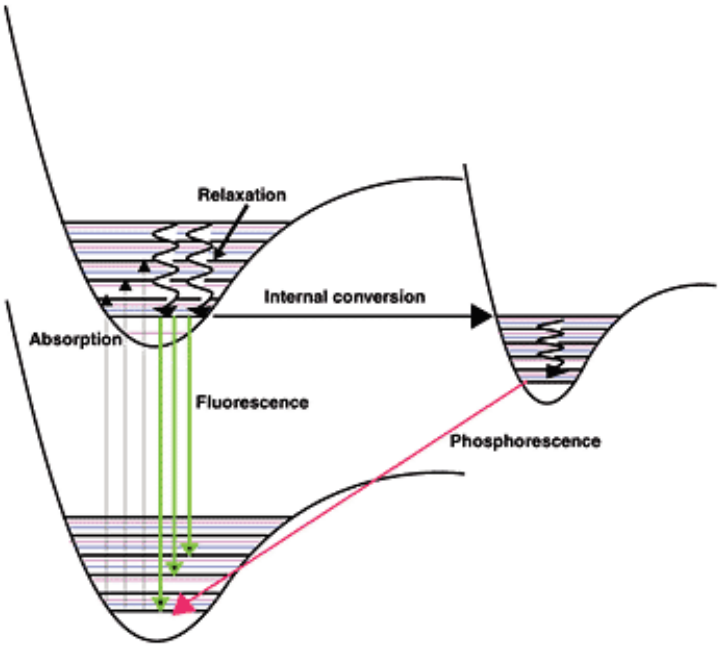

Figure 4. Jablonski diagram showing fluorescence and phosphorescence

An excited chromophore is very likely to relax non-radiatively to the vibrational ground of electronic excited state prior to the luminescence. This loss of energy, shown with squiggly arrows in Figure 4, causes a red-shifted emission spectrum when compared to the absorption spectrum and called Stokes shift[18].

Most important characteristics of a fluorophore, perhaps, are wavelength of the absorption maximum, quantum yield and lifetime. Absorption maximum is directly dependent on energy difference between excited and ground states. Energy difference can be engineered by means of chemical modification on the fluorophore, at least to some level. Also non-covalent and reversible interactions can be used to modulate absorption/emission wavelength.

Quantum yield is defined as the fraction of photons re-emitted after being absorbed. Higher quantum yield means higher intensity, i.e.brighter fluorescence. If designed properly, intensity of fluorophores can also be controlled very efficiently –usually on-off type control can be achieved. These

modulation mechanisms are very common in fluorescent logic gates and will be covered briefly.

1.2.3 Photoinduced Electron Transfer

In certain cases, before relaxation occurs, excited molecule can transfer an electron from some potential donor to fill its low-lying empty orbital. This process has been studied well due to its major role in photosynthesis[20] and is called photoinduced electron transfer (*PeT*).

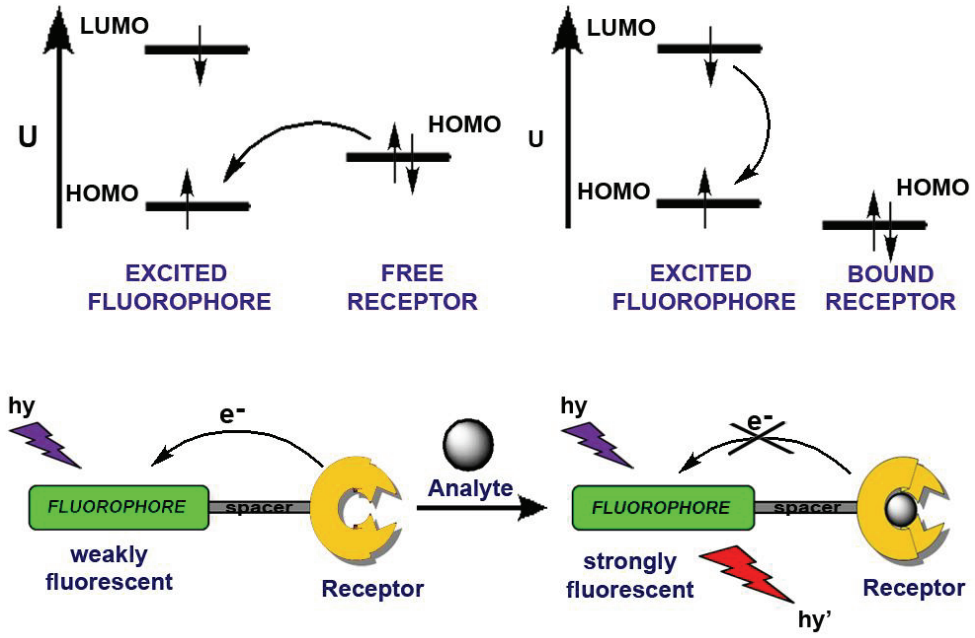

Figure 5. Schematical representation that shows reversible control of PeT process, hence fluorescence

Photoinduced electron transfer blocks the usual relaxation pathway of excited fluorophore and quenches emission. If PeT-donor orbital that gave electron to the excited fluorophore can be controlled (i.e. somehow stabilized to make PeT thermodynamically less favored and destabilized again), an on-off type control over the fluorescence emission will be gained. Accordingly, architectures that

integrate a fluorophore and a PeT-donor receptor used widely in chemosensor designs[21-25] (Figure 5).

In one of these works[23], presented by Akkaya, a bodipy fluorophore is attached to calix[4]arene unit, which is a PeT-donor due to oxygen lone-pairs. Upon protonation of these oxygens, PeT is made less favorable. Thus more than 10-fold change in fluorescence signal is observed with changing pH. (Figure 6)

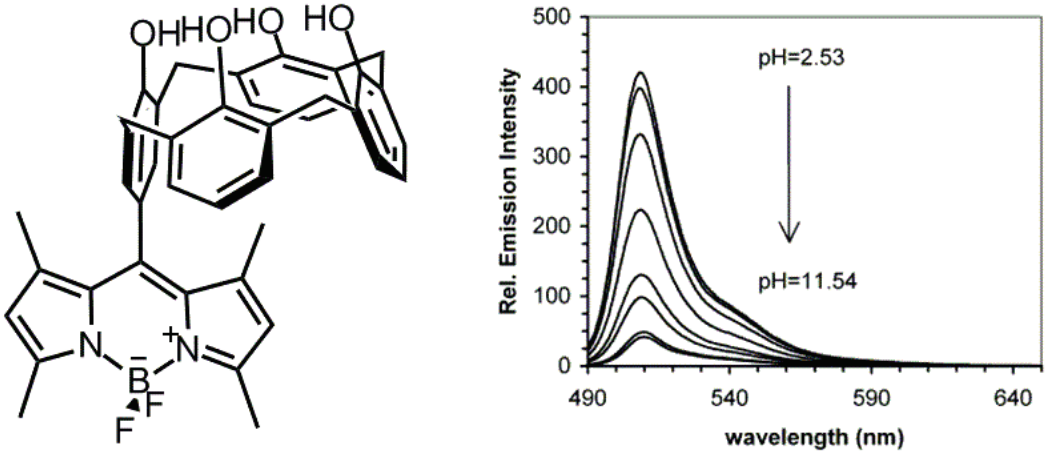

Figure 6. Fluorescence intensity of Bodipy is controlled via a pH sensitive PeT donor

Another example[22], reported by Nagano, contains a slightly different mechanism of PeT, called donor-excited PeT (d-PeT). In this mechanism, electron transfer occurs from excited fluorophore to some empty orbital of an acceptor, in contrast with the usual PeT mechanism (Figure 7). Nagano's work is a thiol sensor, which utilizes a maleimide moiety as PeT acceptor and bodipy as the fluorophore again. Maleimide reacts with thiols irreversibly and 350-fold increase in fluorescence signal achieved.

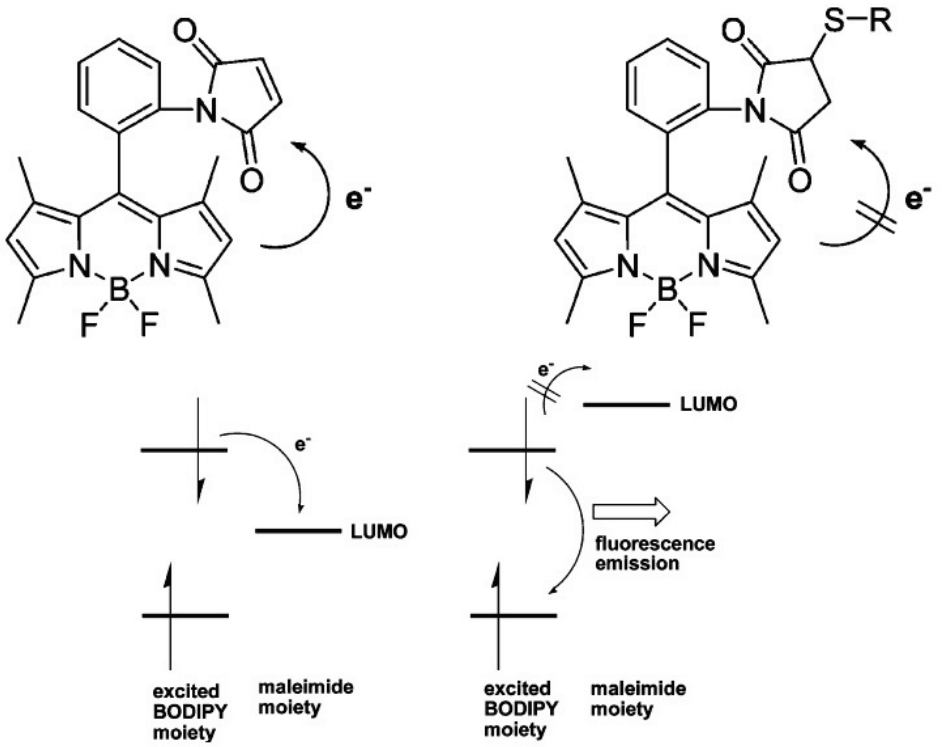

Figure 7. Reverse PeT (d-PeT) mechanism can also be used in the same manner

Synthesizing also meta- and para-maleimide bound structures, Nagano group studied the effect of distance between donor and acceptor on PeT efficiency. O-maleimide came out to be 185 times more efficient PeT acceptor than meta-maleimide and 270 times more efficient then para-maleimide[22].

Photoinduced electron transfer drew attention since it can be controlled by reversible interactions and provides a sharp change in emission intensity that is virtually an on-off type of control.

1.2.4 Internal Charge Transfer

Another mechanism used to manipulate fluorescence characteristics of a fluorophore is called Internal Charge Transfer (ICT). Principles of ICT were first appeared[26] in effort of rationalizing increased acidity of phenol. However, until Valeur[27-29], generalization of these ideas and systematic exploitation in

metal-sensing was not realized. ICT caused by solvent – chromophore interactions has been studied widely. In this study, however, it will be omitted and focus will be given on the applications of ICT in ion sensing phenomena only. As pictured in Figure 8 in a simplified manner, analyte binding can cause different energetic behavior in ground and excited states, and in turn spectral shifts, due to dipole moment change of the fluorophore upon excitation.

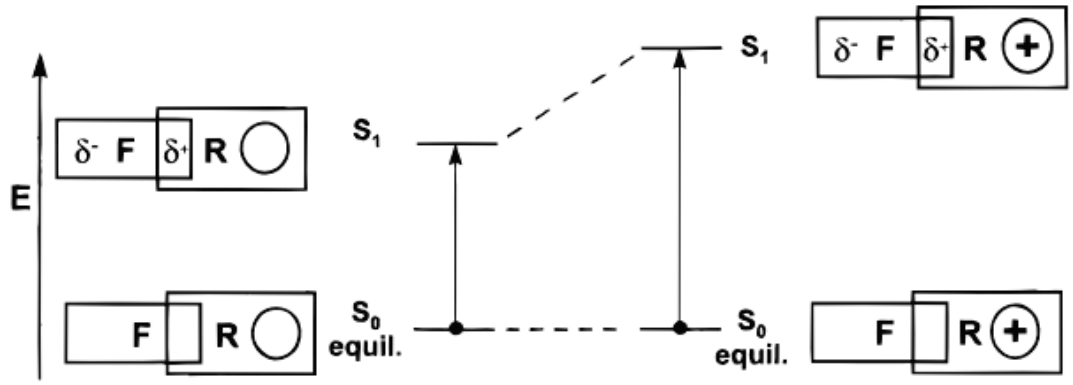

Figure 8. Dipole moment change upon excitation effects the interaction of molecule with charged or polar species

Spectral shift can be bathochromic or hypsochromic depending on the nature of supramolecule. In 2008, Akkaya et al. reported[30] two similar structures based on bodipy dyes, which responds in an opposite direction upon proton binding. This contradiction is based upon a clever design trick: As shown in Figure 9, one of these molecules contain aniline moiety as receptor, which is an electron donor in its free form while other contains pyridine a rather electron-withdrawing moiety. Hence, two molecules have dipole moments pointing opposite directions in excited state and behave oppositely in their bound form.

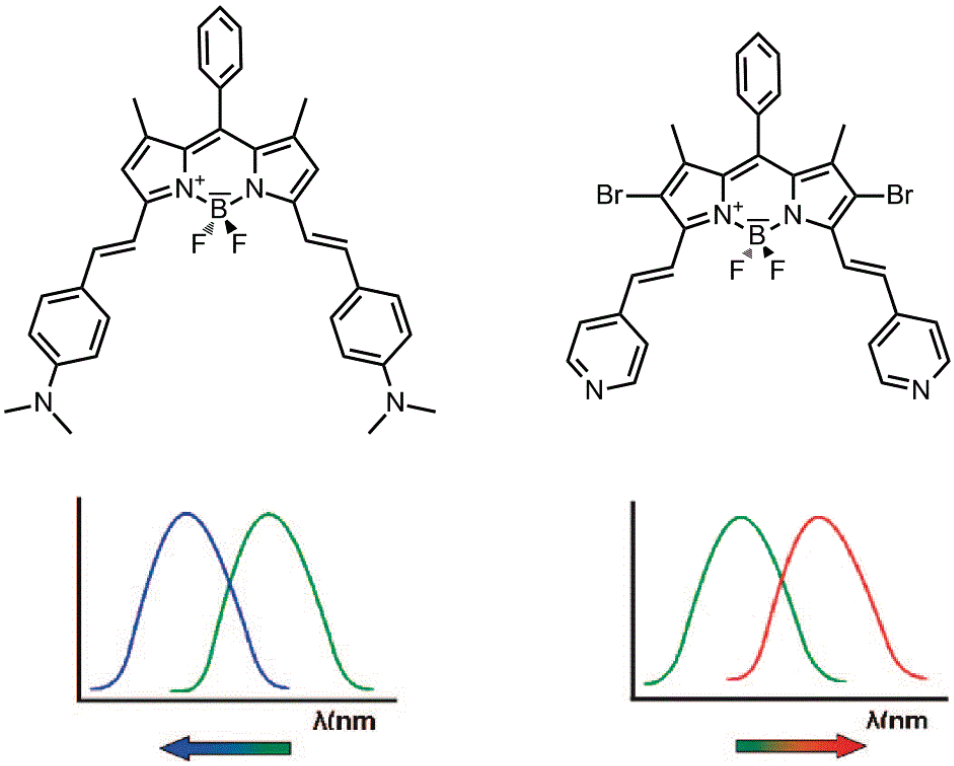

Figure 9. ICT mechanism can be used to generate both blue and red shifts in spectra

A spectral shift caused by ICT is not "as digital as" blocking and unblocking of an emission via PeT, at least at first glance. That's why most of the successful logic systems functioned via PeT until Akkaya's work[31] at *Organic Letters* broke the monopoly and yielded[32] the idea of *wavelength-reconfigurable* logic gates.

1.2.5 Basic Logic Gates at Molecular Level

Information processing at molecular level requires molecules that perform logic operations. This requirement attracted interest of scientists, especially in the last two decades. Since the aforementioned first achievement[17] of de Silva, many other systems have been designed that perform most simple logic operations[33-36]. In this section **AND**, **OR**, INHIBIT (**INH**) and exclusive **OR** (**XOR**) gates will be introduced with examples from literature.

1.2.5.1 AND Gate

An **AND** logic is one that gives an output signal if and only if both two of the inputs are positive. There are many published examples[37-46] of molecular **AND** gates in the literature. One example for this gate is shown in Figure 10 from de Silva's work[44].

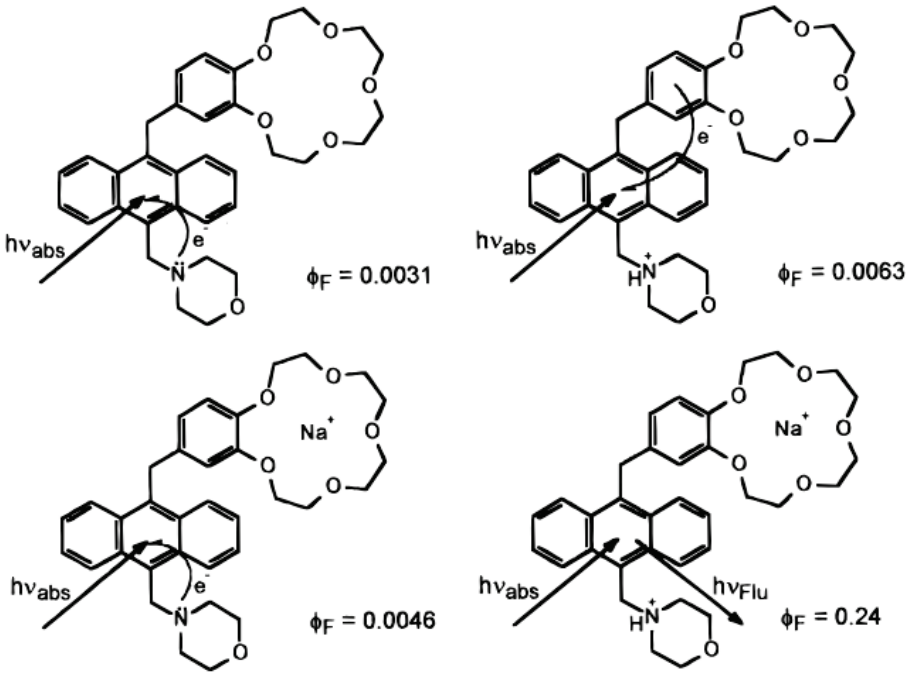

Figure 10. An anthracene based **AND** gate

In this particular example, anthracene chromophore is installed with two different PeT donors, one of which senses proton and other Na^+ cations. Only in the presence of both proton and Na^+/K^+ cations, PeT pathways for both of these donors are blocked and fluorescence emission above a threshold is observed.

1.2.5.2 OR Gate

OR gate, which responds two different targets in the same way, is probably the easiest one to be implemented chemically. Truth table for the **OR** gate is shown below (Table 2).

Table 2. Truth table for the **OR** logic

INPUT 1	INPUT 2	OUTPUT
0	0	0
0	1	1
1	0	1
1	1	1

An example[47] of molecular **OR** gate is shown in Figure 11 that works on the basis of PeT phenomenon. Tricarboxylic acid moiety can bind virtually non-selectively to Ca^{2+} and Mg^{2+} cations which constitutes **OR** characteristic of fluorescence emission.

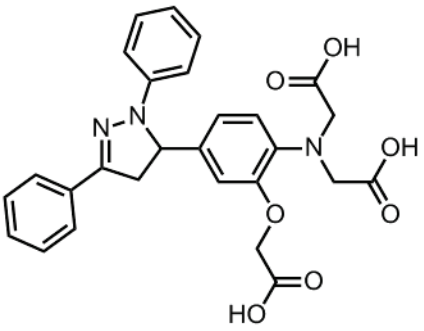

Figure 11. Non-selectivity is used to design an **OR** gate

1.2.5.3 Inhibit (INH) Gate

In the inhibit logic, output signal can be inhibited by one of the inputs. This logic demonstrates non-commutative behavior –gate responds asymmetrically to the inputs- and can be obtained using a **NOT** and a **AND** gate. Table 3 shows the truth table for **INH** gate.

Table 3. Truth table for **INH** gate

INPUT 1	INPUT 2	OUTPUT
inhibitor	input	output
0	0	0
1	0	0
0	1	1
1	1	0

One[48] of the many examples[48-55] of published **INH** gates is shown in Figure 12 with relevant photophysical processes. In this work of Pischel group, luminescence Eu^{3+} is monitored as output signal. Eu^{3+} has a low extinction coefficient but can be efficiently excited by energy transfer from triplet state of amino-substituted 1,8-naphthalimide. In the presence of O_2, concerning triplet state is quenched before it transfers energy to Eu^{3+} cation and luminescence is inhibited. It is interesting to note that Eu^{3+} cation itself, which is the source of luminescence, is assigned as one of the inputs.

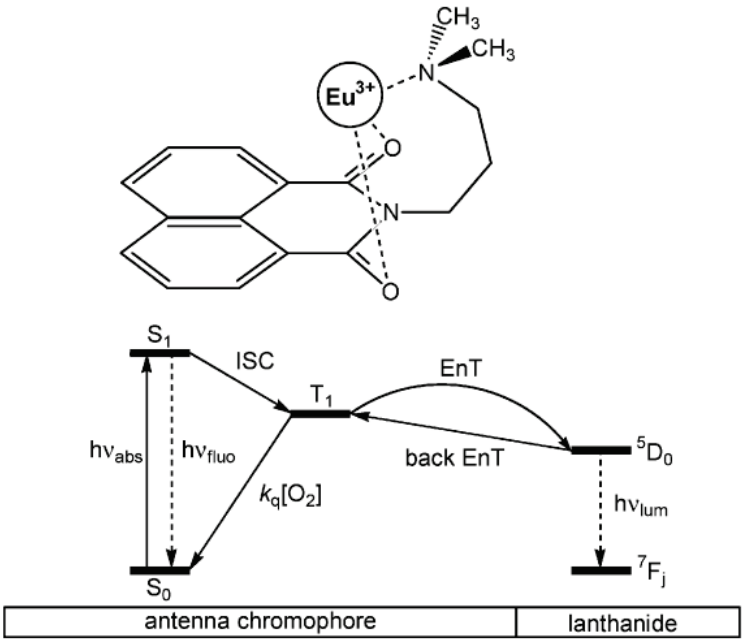

Figure 12. Possible relaxation pathways for concerning **INH** gate

1.2.5.4 Exclusive OR (XOR) Gate

Exclusive **OR** gate acts in the same way as the logical "either": there is an output signal if either, but not both, of the inputs are present. Another way of looking at this logic element is to say that there is an output only if two inputs are different (Table 4).

Table 4. Truth table for **XOR** gate

INPUT 1	INPUT 2	OUTPUT
0	0	0
0	1	1
1	0	1
1	1	0

XOR behavior is one of the hardest logic behaviors to mime at molecular level. There are several literature examples[56-58] that are not a single molecule but a mixture or a supramolecular assembly. Also using two annihilating inputs –such as acid and base- is a common trick[59-63] of architecturing a molecular **XOR** gate. De Silva group, again, achieved the first single-molecular **XOR** gate[64] that is not based on annihilation of inputs. Their design, shown in Figure 13, contains four carboxylic acid groups capable of binding Ca^{2+} and a pyridine moiety that binds to proton. Effects of Ca^{2+} and H^{+} addition, to the absorption spectrum, via ICT are also shown in Figure 13.

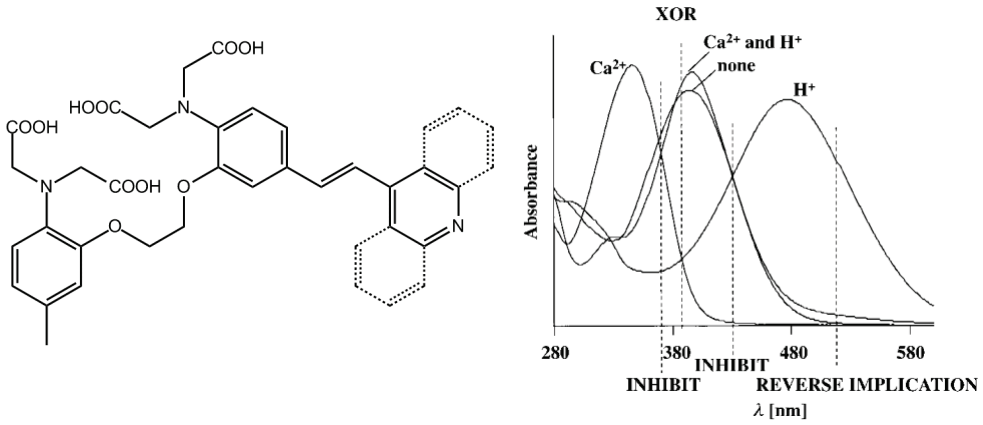

Figure 13. First **XOR** gate not relying on annihilating inputs along with the absorption spectrum

1.2.6 Towards and Beyond the Molecular Arithmetics

Implementing basically all logic operations chemically raised the bar of expectation for more complex digital operations. Most obvious operation of that kind is arithmetic processing of binary data and performed by half-adders and half substractors.

1.2.6.1 Molecular Half-Adder

A half-adder[65-73] performs addition of two bits and can be obtained by concatenation of an **AND** gate and an **XOR** gate working in parallel. Truth table for this operation is shown in **Table 5**.

Table 5. Truth table for a half-adder

INPUT		OUTPUT	
1	2	AND	XOR
0	0	0	0
0	1	0	1
1	0	0	1
1	1	1	0

First molecular half-adder, is reported[74] by de Silva in 2000. In this work, rather than combining two gates in a molecule or in a supramolecule, two molecules which separately mimic **AND** and **XOR** logics used in a mixture.

In 2005, Shanzer group published[75] first unimolecular example of half-adder on a surprisingly simple platform: fluorescein. Different protonation states of the fluorescein molecule (shown in Figure 14) exhibit significant spectral differences. This provide the possibility for extraction of various gate behaviours from distinct parts of spectrum (i.e. wavelength-reconfigurable logic, defined in section Internal Charge Transfer). In the mentioned work, Shanzer and coworkers demonstrated that absorption spectrum of fluorescein exhibits **XOR** behavior at 447 nm and **AND** behavior at 501 nm.

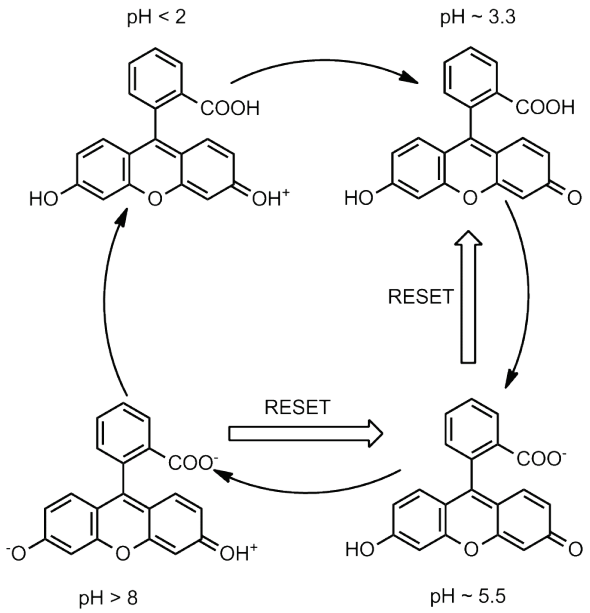

Figure 14. First molecular half-adder

1.2.6.2 Half-Substractor

Another obvious arithmetic operation, taking difference of two bits, is performed by half-substractor (Table 6). A half-substractor also can be obtained by two parallel working simple logic gates, **INH** and **XOR** gates this time.

Table 6. Truth table for a half-substractor

INPUT		OUTPUT	
1	2	INH	XOR
0	0	0	0
0	1	1	1
1	0	0	1
1	1	0	0

First[76] of many molecular half-substractor examples[77-81] is achieved in Langford Laboratory. Langford and coworkers studied tetraphenylporphyrin as the gate, and used acid-base annihiliating inputs. Soret band of porphyrine localized at 417 nm shifts above 425 nm in presence of acid or base, hence exhibits **XOR** behavior. On the other hand cationic form –which exists in acidic media- is strongly fluorescent at 405 nm. This emission can be read as **INH** gate.

Full-adders and full-substractors take three input, yield two output bits and fundemantally achieve the highest complexity of arithemetic operations. There are several published examples[82-85] of those kind molecular devices operating on the same basis. Molecular keypad lock[86], multiplexer[87] – demultiplexer[88], sequential logic and molecular information storage[89,90] are several other examples of studied so far.

Chemical input-optical output has a widespread use in molecular logic gate designs. Nevertheless, there are chemical input-chemical output, optical input-optical output (all photonic) gates also. These works are comprehensively reviewed[33-36,91-93] by several different groups.

1.2.7 Ready-to-use implications of Molecular Logic

Mostly due to input-output heterogeneity and difficulties in individual addressability, integration of molecular logic gates to perform more complex digital operations is still a problem. According to Akkaya, however, "it may be challenging to integrate two molecular logic gates; however, they can be easily integrated into the control processes of healthy or pathological biochemistry". Pointing this out, in his communication paper[4] published in 2008 he claims "chemical logic systems are inherently more capable than they are given credit for, and, the potential of the chemical logic gates is yet largely untapped".

One of the early ideas on this subject emerged in a 2005 paper[94] of de Silva published in the Journal of the American Chemical Society. In his paper, de Silva, suggested a three input **AND** gate (Figure 15) in which an anthracene moiety is used as the fluorophore and a benzo-15-crown-5, a tertiary amine and a phenyliminodiacetate are used as PeT donor receptors, to signal Na^+, H^+ and Zn^{2+}, respectively. The idea debuted in this work is that, such a design can be considered as a *"lab-on-a-molecule"*, which responds to threshold values to three different symptoms of a disease. That would replace three separate clinical tests and their analysis with a single and simple test.

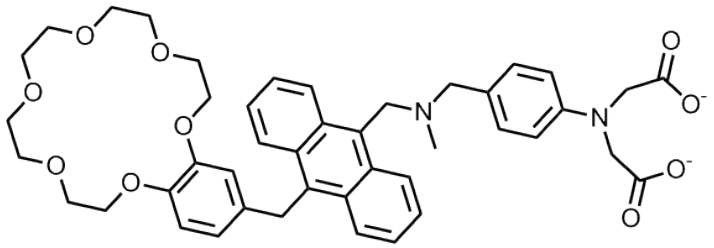

Figure 15. Lab-on-a-molecule idea demonstrates a striking application for molecular logic

Same year, Shabat and coworkers published[5] an **OR** gate-implemented prodrug

(Figure 16), which releases the active anticancer drug doxorubicin in presence of *antibody 38C2* or *penicillin G amidase*. It is interesting to note that output of this molecular logic device is also chemical: a molecule of doxorubicin.

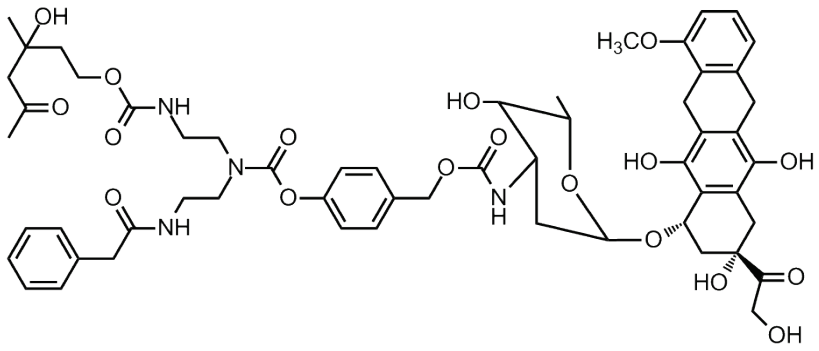

Figure 16. OR logic based drug release

A recent work is aforementioned paper[4] of Akkaya, in which an **AND** gate implemented *photodynamic therapy reagent* has been debuted. This reagent (Figure 17) produces singlet O_2 sensitive to Na^+ (which blocks PeT donor tethered at *meso* position) and H^+ (which causes a red shift via ICT mechanism) concentrations which is high in tumor cells.

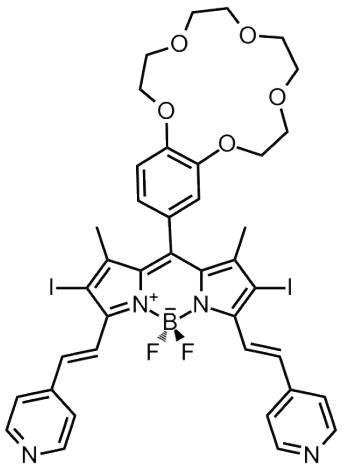

Figure 17. A photodynamic therapy reagent controlled by an **AND** logic

CHAPTER 2

EXPERIMENTAL PROCEDURES

2.1 General

^{1}H NMR and ^{13}C NMR spectra were recorded on Bruker DPX-400 (operating at 400 MHz for ^{1}H NMR and 100 MHz for ^{13}C NMR) in $CDCl_3$ with tetramethylsilane as internal standard. All spectra were recorded at 25 ^{o}C and coupling constants (*J* values) are given in Hz. Chemical shifts are given in parts per million (ppm). All the ^{13}C spectra were recorded with simultaneous decoupling of proton nuclei. Mass spectroscopy data were acquired using Bruker Autoflex-III (smartbeam) MALDI TOF/TOF system at IYTE Chemistry Department, Izmir, Turkey. Varian Cary-100 spectrophotometer is used to record absorption spectra. For fluorescence measurements Varian Eclipse spectrofluorometer was used. Reactions were monitored by thin layer chromatography using Merck TLC Silica gel 60 F_{254}. Silica gel column chromatography was performed over Merck Silica gel 60 (particle size: 0.040-0.063 mm, 230-400 mesh ASTM). All other reagents and solvents were purchased from Aldrich and used without further purification. 4,4-difluoro-8-phenyl-1,3,5,7-tetramethyl-4-bora-3a,4a-diaza-*s*-indacene[95] and 4-(1,4-dioxa-7,13-dithia-10-azacyclopentadecan-10-yl) benzaldehyde[96] were synthesized according to literature. Isothermal titration calorimetry experiments were performed on a iTC-200 microcalorimeter (Microcal Inc., Northampton, MA). All solutions were prepared in spectroscopic grade CH_3CN. For a typical ITC run, the instrument chamber (200 μL) contained a solution of a ligand (0.1 – 0.5 mM) while a 1.0 – 5.0 mM solution of $Zn(ClO_4)_2$ or $Hg(ClO_4)_2$ was taken up in a 40 μL injection syringe. The syringe was assembled into the chamber for equilibration while stirring at 1000 rpm. The chamber temperature was set to 25 °C. The injections were programmed at 1 μL each, added over 2 sec and spaced 2 min apart. Association enthalpy (ΔH° in cal/mol), "number of sites" (N), and

association constant (K in M^{-1}) were obtained by fitting the titration data using the "One (Two) Set of Sites model" algorithm provided in the MicroCal Origin Software package (version 7.0). Association entropy (ΔS in cal/mol K) is calculated from fitted values of ΔHº and K.

2.2 Synthesis of target molecule 2

2.2.1 Synthesis of Compound 1.

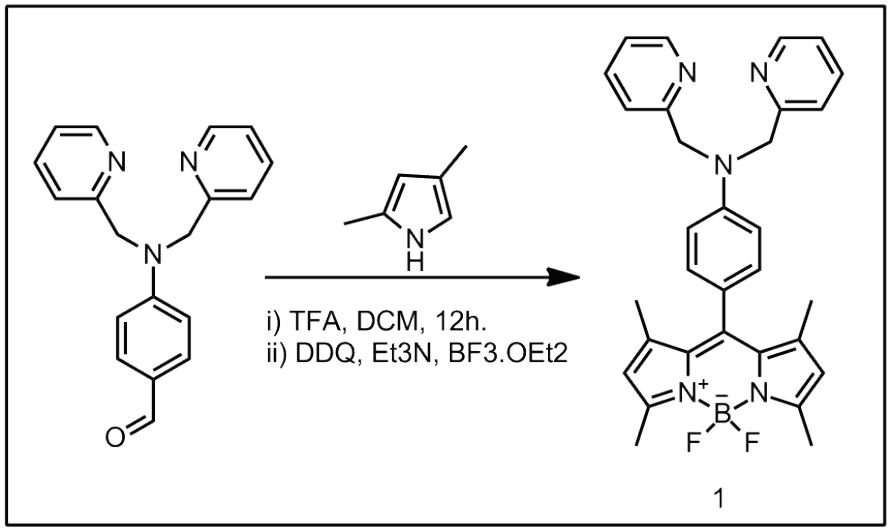

Figure 18. Synthesis of compound **1**

To a 1.0 L round-bottomed flask containing 400 mL argon-degassed CH_2Cl_2 2,4-dimethyl pyrrole (4.4 mmol, 0.4 g), 4-(*N,N*-di-(pyridine-2-ylmethyl)amino) benzaldehyde[95] (1.98 mmol, 0.6 g) and one drop of trifluoroacetic acid were added. The solution was stirred under N_2 at room temperature for 1 day. After addition of a solution of DDQ (1.98 mmol, 0.45 g) in 100 mL of CH_2Cl_2 to the reaction mixture, stirring was continued for 30 min. 6 mL of Et_3N and 5 mL of $BF_3{\cdot}OEt_2$ were successively added and after 30 min, the reaction mixture was washed with water (3 x 300 mL) and dried over anhydrous Na_2SO_4. The solvent was evaporated and the residue was purified by silica gel column chromatography using $CHCl_3$: Methanol (97 : 5) as the eluant. Orange solid

(0.25 g, 23%). ^{1}H NMR (400 MHz, $CDCl_3$): δ_H 8.60 (2H, d, *J* = 6.48 Hz, ArH), 7.62 (2H, t, *J* = 7.71 Hz, ArH), 7.22 (2H, d, *J* = 7.84 Hz, ArH), 7.18 (2H, t, *J* = 6.58 Hz, ArH), 6.98 (2H, d, *J* = 8.80, ArH), 6.80 (2H, d, *J* = 8.80, ArH), 5.95 (2H, s, ArH), 4.87 (4H, s, CH_2), 2.52 (6H, s, CH_3), 1.45 (6H, s, CH_3); ^{13}C NMR (100 MHz, $CDCl_3$): δ_C 158.3, 154.8, 149.8, 149.7, 148.8, 143.1, 136.7, 128.9, 123.3, 122.2, 120.9, 113.2, 57.4, 14.5 ppm. Anal. Calcd. for $C_{31}H_{30}BF_2N_5$: C 71.41, H 5.80, N 13.43. Found: C 71.33, H 5.89, N 13.12 %.

2.2.2 Synthesis of Compound 2.

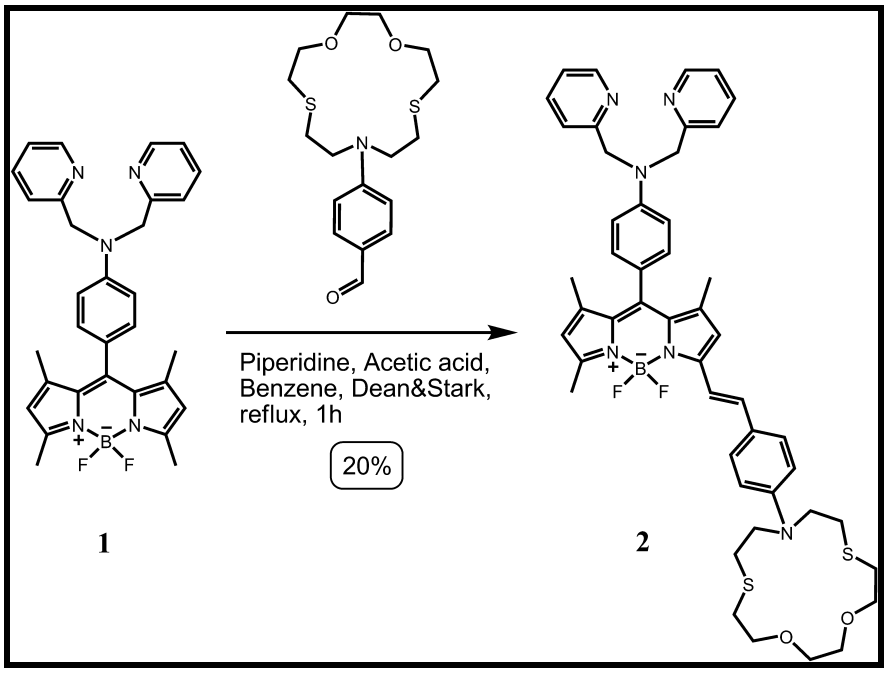

Figure 19. Synthesis of compound **2**

40 mL of benzene, compound **1** (0.15 mmol, 80 mg), 4-(1,4-dioxa-7,13-dithia-10-azacyclopentadecan-10-yl) benzaldehyde[95] (0.15 mmol, 54 mg), acetic acid (0.2 mL), and piperidine (0.2 mL) were mixed in a 100 mL round-bottomed flask and refluxed with Dean-Stark apparatus. Reaction mixture was stirred almost until all solvent evaporized. Progress of the reaction was monitored by TLC (1:1 Hexanes : Acetone). After consumption of starting materials, water (100 mL) was added and mixture was extracted into $CHCl_3$. Organic layer was

dried on Na_2SO_4 and evaporated. Column chromatographic separation (silica gel, 1:1 Hexanes : Acetone) of the residue yielded the desired product as a dark blue solid. (25 mg, 20%). ^{1}H NMR (400 MHz, $CDCl_3$): δ_H 8.62 (2H, d, *J* = 5.72 Hz, ArH), 7.65 (2H, t, *J* = 8.54 Hz, ArH), 7.50-7.43 (3H, m: 2H, ArH; 1H, C*H*), 7.26-7.15 (5H, m: 4H, ArH; 1H, C*H*), 7.03 (2H, d, *J* = 8.60 Hz, ArH), 6.80 (2H, d, *J* = 8.68 Hz, ArH), 6.62 (2H, d, *J* = 8.96, ArH), 6.58 (1H, s, ArH), 5.90 (1H, s, ArH), 4.88 (4H, s, CH_2), 3.82 (4H, t, *J* = 4.98 Hz, OCH_2CH_2S), 3.70-3.62 (8H, m, 4H, NCH_2CH_2S, 4H, OCH_2CH_2O), 2.90 (4H, t, *J* = 7.86 Hz, OCH_2CH_2S), 2.78 (4H, t, *J* = 5.05 Hz, NCH_2CH_2S), 2.58 (6H, s, CH_3), 1.48 (3H, s, CH_3), 1.44 (3H, s, CH_3); ^{13}C NMR (100 MHz, $CDCl_3$): δ_C 158.4, 153.0, 149.8, 149.0, 148.7, 139.0, 136.7, 129.5, 129.3, 126.0, 125.2, 122.1, 120.9, 120.7, 117.0, 115.0, 113.1, 111.8, 74.3, 70.7, 57.5, 51.9, 31.3, 29.6, 14.8, 14.7 ppm. Anal. Calcd. for $C_{48}H_{53}BF_2N_6O_2S_2$: C 67.12, H 6.22, N 9.78 %. Found: C 66.98, H 6.34, N 9.70 %. MS (MALDI-TOF): m/z: Calcd. For $C_{48}H_{53}BF_2N_6O_2S_2$: 858.4 [$M^+$], Found: 858.1[$M^+$].

2.3 Synthesis of Half adder 4.

2.3.1 Synthesis of Compound 3.

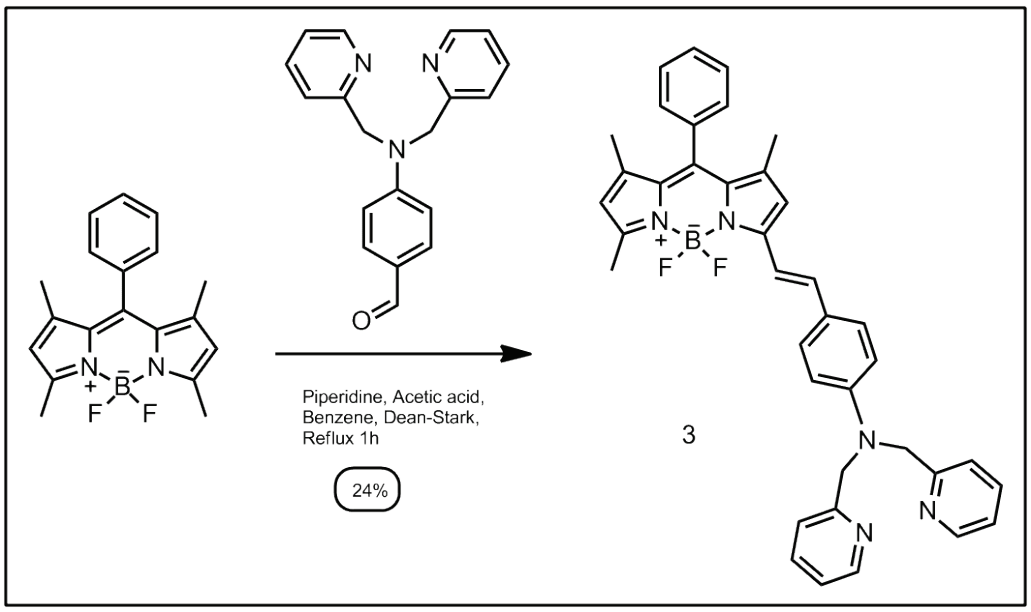

Figure 20. Synthesis of compound **3**

40 mL of benzene, 4,4-difluoro-8-phenyl-1,3,5,7-tetramethyl-4-bora-3a,4a-diaza-*s*-indacene (0.37 mmol, 0.12 g), 4-(*N,N*-di-(pyridine-2-ylmethyl)amino) benzaldehyde[95] (0.37 mmol, 0.11 g), acetic acid (0.2 mL), and piperidine (0.2 mL) were mixed in a 100 mL round-bottomed flask and refluxed with Dean-Stark apparatus. Reaction mixture was stirred almost until all solvent evaporized. Progress of the reaction was monitored by TLC (Ethyl acetate : Methanol ; 97:3). After consumption of starting materials, water (100 mL) was added and mixture was extracted into $CHCl_3$. Organic layer was dried on Na_2SO_4 and evaporated. Column chromatographic separation (silica gel, Ethyl acetate : Methanol ; 97 : 3) of the residue yielded desired product as a dark blue solid (53mg, 24%). ^{1}H NMR (400 MHz, $CDCl_3$): δ_H 8.61 (2H, d, J = 5.72 Hz, ArH), 7.65 (2H, t, J = 8.48 Hz, ArH), 7.50-7.40 (6H, m: 3H, ArH; 2H, ArH; 1H, C*H*), 7.30-7.22 (4H, m: 2H, ArH; 2H, ArH), 7.20-7.12 (3H, m: 2H, ArH; 1H, C*H*), 6.72 (2H, d, J = 8.21 Hz, ArH), 6.57 (1H, s, ArH), 5.95 (1H, s, ArH), 4.88

(4H, s, CH_2), 2.55 (6H, s, CH_3), 1.41 (3H, s, CH_3), 1.39 (3H, s, CH_3); ^{13}C NMR (100 MHz, $CDCl_3$): δ_C 158.9, 158.2, 154.3, 153.5, 149.8, 149.7, 142.7, 141.3, 139.2, 136.9, 136.8, 135.3, 129.2, 129.0, 128.8, 125.9, 122.2, 122.0, 120.8, 117.6, 117.2, 115.3, 112.7, 57.3, 14.6, 14.5, 14.2 ppm. Anal. Calcd. for $C_{38}H_{34}BF_2N_5$: C 74.88, H 6.62, N 11.49 %. Found: C 74.91, H 6.73, N 11.40 %. MS (MALDI-TOF): m/z: Calcd. For $C_{38}H_{34}BF_2N_5$: 609.3 [M^+], Found: 608.9 [M^+].

2.3.2 Synthesis of Compound 4.

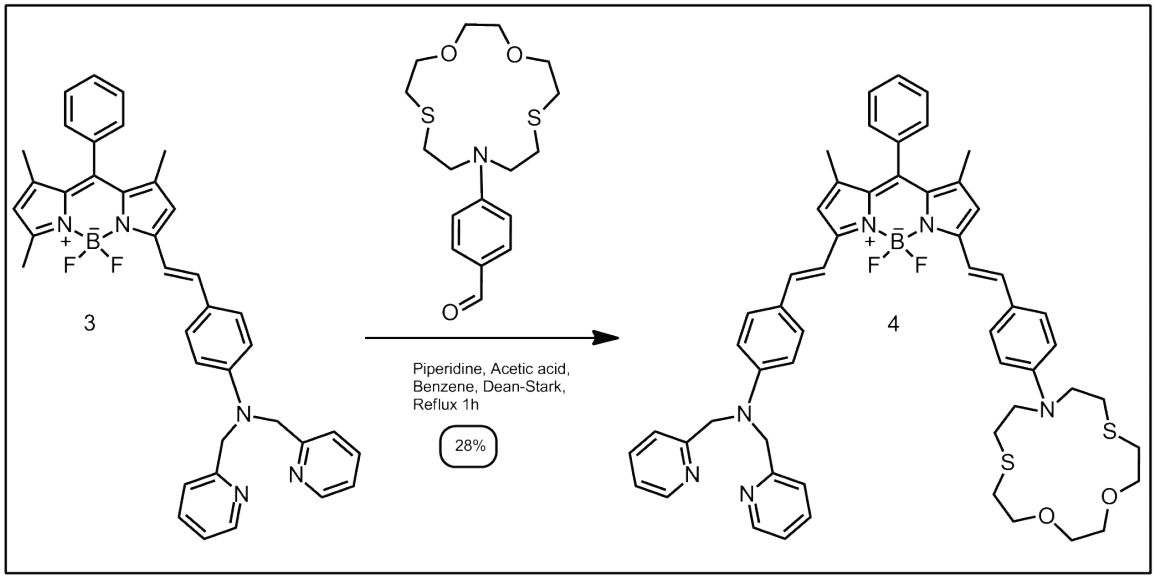

Figure 21. Synthesis of compound **4**

40 mL of benzene, 3 (0.08 mmol, 50 mg), 4-(1,4-dioxa-7,13-dithia-10-azacyclopentadecan-10-yl) benzaldehyde[96] (0.08 mmol, 28.4 mg), acetic acid (0.2 mL), and piperidine (0.2 mL) were mixed in a 100 mL round-bottomed flask and refluxed with Dean-Stark apparatus. Reaction mixture stirred almost until all solvent evaporized. Progress of the reaction was monitored by TLC (Ethyl acetate : Methanol ; 95:5). After consumption of starting materials, water (100 mL) was added and mixture was extracted into $CHCl_3$. Organic layer was dried on Na_2SO_4 and evaporated. Column chromatographic separation (silica gel, Ethyl acetate : Methanol ; 95 : 5) of the residue yielded the desired product

as a green solid. (25 mg, 28%). ^{1}H NMR (400 MHz, $CDCl_3$): δ_H 8.63 (2H, d, *J* = 3.16 Hz, ArH), 7.67 (2H, t, *J* = 7.26 Hz, ArH), 7.58-7.44 (9H, m: 3H, ArH; 2H, ArH; 2H, ArH; 2H, C*H*), 7.35-7.28 (3H, m: 2H, ArH; 1H, C*H*), 7.24-7.13 (4H, m: 2H, ArH; 2H, ArH), 7.05 (1H, d, *J* = 15.3 Hz, C*H*), 6.74 (2H, d, *J* = 8.40 Hz, ArH), 6.65 (2H, d, *J* = 8.45, ArH), 6.59 (1H, s, ArH), 6.57 (1H, s, ArH), 4.90 (4H, s, CH_2), 3.74 (4H, t, *J* = 4.62 Hz, OCH_2CH_2S), 3.75-3.62 (8H, m, 4H, NCH_2CH_2S, 4H, OCH_2CH_2O), 2.92 (4H, t, *J* = 3.88 Hz, OCH_2CH_2S), 2.78 (4H, t, *J* = 4.50 Hz, NCH_2CH_2S), 2.58 (6H, s, CH_3), 1.42 (6H, s, CH_3); ^{13}C NMR (100 MHz, $CDCl_3$): δ_C 158.3, 153.1, 152.3, 149.9, 149.7, 148.7, 147.6, 141.2, 140.8, 136.9, 136.5, 136.3, 135.6, 135.5, 129.4, 129.1, 128.9, 128.6, 126.3, 125.2, 124.8, 122.6, 122.2, 122.9, 117.3, 117.1, 115.8, 115.0, 112.7, 112.0, 111.8, 74.3, 70.7, 57.3, 52.0, 31.3, 29.7, 14.6, 14.5 ppm. Anal. Calcd. for $C_{55}H_{57}BF_2N_6O_2S_2$: C 69.75, H 6.07, N 8.87 %. Found[97]: C 69.68, H 6.15, N 8.79 %. MS (MALDI-TOF): m/z: Calcd. For $C_{55}H_{57}BF_2N_6O_2S_2$: 946.4 [$M^+$], Found: 946.2 [$M^+$].

2.4 Synthesis of Three Input AND Logic 7.

2.4.1 Synthesis of 4-(1,4,7,10-tetraoxa-13-azacyclopentadecan-13-yl)benzaldehyde

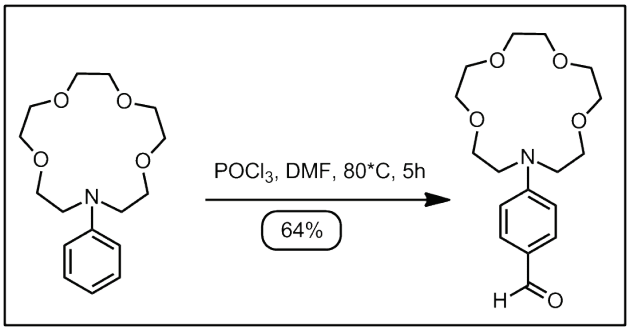

Figure 22. Synthesis of Ca^{2+} ligand tethered benzaldehyde

To a cooled (0°C) solution of anhydrous DMF (10mL), 4 mmol $POCl_3$ (0.615 g) was added within 5 min. The mixture was stirred for 30 min at room temperature, then 13-phenyl-1,4,7,10-tetraoxa-13-azacyclopentadecane[98] (3.4 mmol, 1 g) was added and the resulting mixture was heated for 5h at 80°C. A dark brown solution formed. Cold water was slowly added onto this solution and then it is neutralized with K_2CO_3. The product was extracted with CH_2Cl_2 and dried over anhydrous Na_2SO_4. The solvent was evaporated and the residue was purified by silica gel column chromatography using $CHCl_3$: Methanol (95: 5) as the eluant. Yellowish viscous liquid (0.7 g, 64%). ^{1}H NMR (400 MHz, $CDCl_3$): δ_H 9.72 (1H, s), 8.78 (2H, d, *J* = 8.84 Hz, ArH), 6.80 (2H, d, *J* = 8.96 Hz, ArH), 3.83 (4H, t, *J*=6.16), 3.70-3.56 (16H, m); ^{13}C NMR (100 MHz, $CDCl_3$): δ_C 190.0, 152.4, 132.0, 125.2, 111.0, 71.2, 70.3, 70.0, 68.1, 52.8 ppm. Anal. Calcd. for $C_{17}H_{25}NO_5$: C 63.14, H 7.79, N 4.33 %. Found: C 63.18, H 7.85, N 4.19 %.

2.4.2 Synthesis of Compound 5

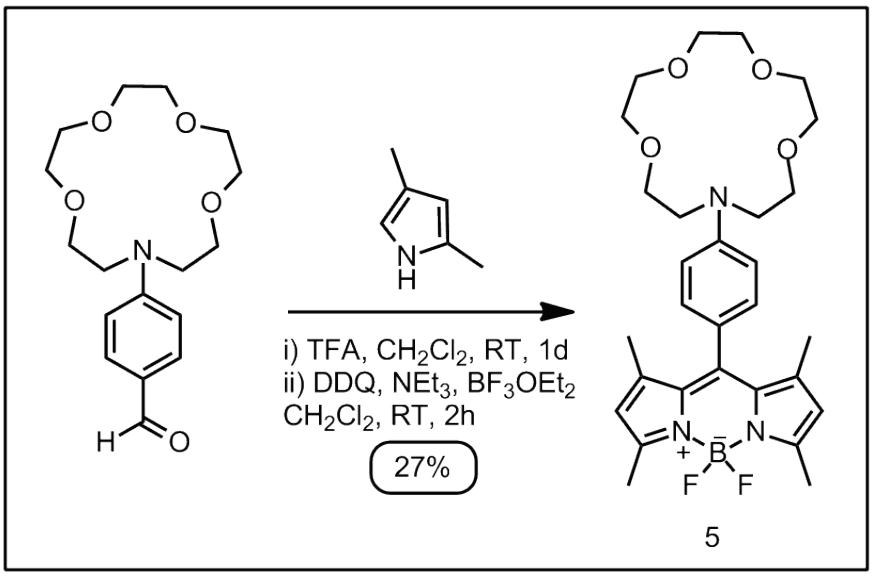

Figure 23. Synthesis of compound **5**

To a 1L round-bottomed flask containing 400 mL argon-degassed CH_2Cl_2 2,4-dimethyl pyrrole (3.41 mmol, 0.324 g), 4-(1,4,7,10-tetraoxa-13-azacyclopentadecan-13-yl)benzaldehyde (1.55 mmol, 0.5 g) and one drop of trifluoroacetic acid were added. The solution was stirred under N_2 at room temperature for 1d. After addition of a solution of DDQ (1.60 mmol, 0.363 g) in 100 mL of CH_2Cl_2 to the reaction mixture, stirring was continued for 30 min. 6 mL of Et_3N and 5 mL of BF_3. Oet_2 were successively added and after 30 min, the reaction mixture was washed with water (3 x 300 mL) and dried over anhydrous Na_2SO_4. The solvent was evaporated and the residue was purified by silica gel column chromatography using $CHCl_3$: Methanol (95 : 5) as the eluant. Orange solid (0.225 g, 27%). ^{1}H NMR (400 MHz, $CDCl_3$): δ_H 7.01 (2H, d, J = 7.92 Hz, ArH), 6.73 (2H, d, J = 8.12 Hz, ArH), 6.94 (2H, s, ArH), 3.80 (4H, t, J=5.64), 3.73-3.60 (16H, m) 2.52 (6H, s, CH_3), 1.50 (6H, s, CH_3); ^{13}C NMR (100 MHz, $CDCl_3$): δ_C 154,7, 148.2, 143.2, 132.2, 130.7, 128.9, 121.8, 120.8, 111.6, 110.7, 71.3, 70.2, 70.0, 68.5, 52.6, 14.8, 14.5 ppm. Anal. Calcd. for $C_{29}H_{38}BF_2N_3O_4$: C 64.33, H 7.07, N 7.76 %. Found: C 64.28, H 7.16, N 7.70 %. MS (MALDI-TOF): m/z: Calcd. For $C_{29}H_{38}BF_2N_3O_4$: 541.3 [M^+], Found: 541.9 [M^+].

2.4.3 Synthesis of Compound 6

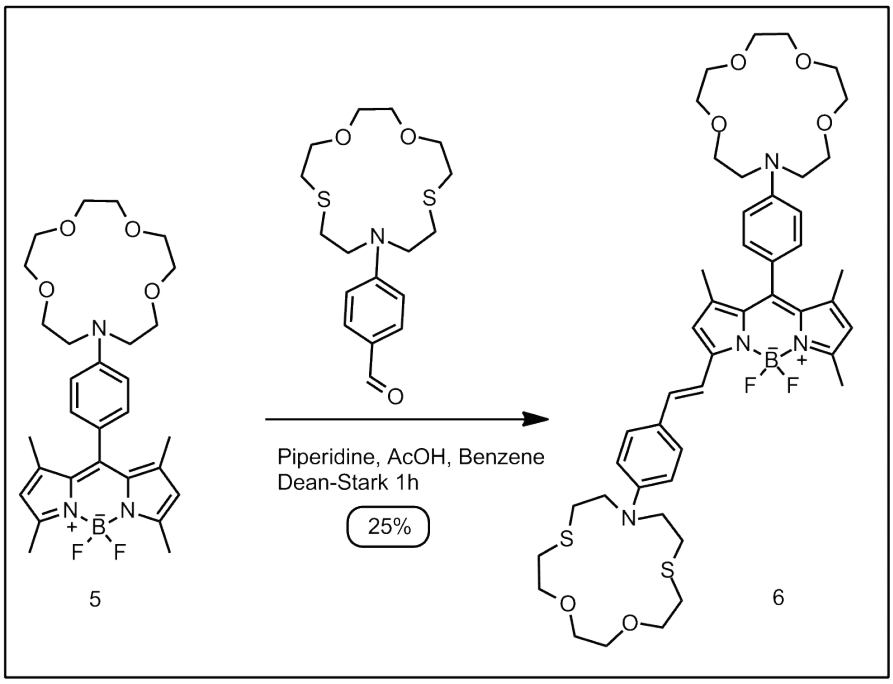

Figure 24. Synthesis of compound **6**

40 mL of benzene, compound **5** (0.37 mmol, 200 mg), 4-(1,4-dioxa-7,13-dithia-10-azacyclopentadecan-10-yl)-benzaldehyde[96] (0.33 mmol, 118 mg), acetic acid (0.2 mL), and piperidine (0.2 mL) were mixed in a 100 mL round-bottomed flask and refluxed with Dean-Stark apparatus. Reaction mixture was stirred almost until all solvent evaporized. Progress of the reaction was monitored by TLC (eluent: Ethyl acetate). After consumption of starting materials, water (100 mL) was added and mixture was extracted into $CHCl_3$. Organic layer was dried on Na_2SO_4 and evaporated. Column chromatographic separation (silica gel, eluent: Ethyl acetate) of the residue yielded the desired product as a dark blue solid. (80 mg, 25%). ^{1}H NMR (400 MHz, $CDCl_3$): δ_H 7.54-7.42 (3H, m: 2H, ArH; 1H, C*H*), 7.18 (1H, d, *J* = 16.10 Hz, CH), 7.05 (2H, d, *J* = 8.60 Hz, Ar*H*), 6.75 (2H, d, *J* = 8.70 Hz, C*H*), 6.62 (2H, d, *J* = 8.90 Hz, ArH), 6.10 (1H, s, ArH), 5.95 (1H, s, ArH), 3.85-3.75 (8H, m), 3.72-3.59 (24H, m), 2.91 (4H, t, *J* =7.80 Hz), 2.78 (4H, t, *J* = 4.90 Hz), 2.57 (3H, s), 1.54 (3H, s), 1.50 (3H, s); ^{13}C NMR (100 MHz, $CDCl_3$): δ_C 154.0, 148.0, 147.6, 142.9, 140.5, 136.7, 130.9,

130.8, 129.7, 129.4, 129.3, 125.0, 123,5 122.2, 120.2, 117.2, 114.8, 111,8, 111.6, 74.2, 71.3, 70.7, 70.2, 70.0, 68.5, 52.6, 51.9, 31.6, 31.3, 30.3, 29.6, 15.1, 14.7 ppm. Anal. Calcd. for $C_{46}H_{61}BF_2N_4O_6S_2$: C 62.86, H 7.00, N 6.37 %. Found: C 63.01, H 7.14, N 6.40 %. MS (MALDI-TOF): m/z: Calcd. For $C_{46}H_{61}BF_2N_4O_6S_2$: 878.4 [$M^+$], Found: 878.2 [$M^+$].

2.4.4 Synthesis of Compound 7

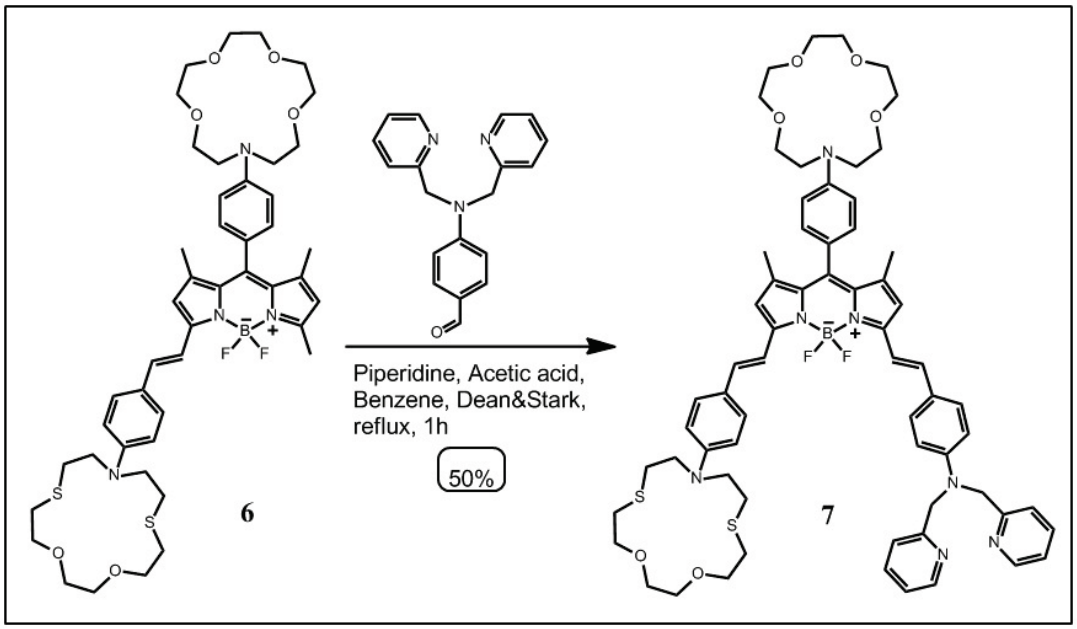

Figure 25. Synthesis of compound **7**

40 mL of benzene, **6** (0.06 mmol, 50 mg), 4-(*N,N*-di-(pyridine-2-ylmethyl)amino)benzaldehyde[95] (0.12 mmol, 36.40 mg), acetic acid (0.2 mL), and piperidine (0.2 mL) were mixed in a 100 mL round-bottomed flask and refluxed with Dean-Stark apparatus. Reaction mixture stirred almost until all solvent evaporized. Progress of the reaction was monitored by TLC (Ethyl acetate : Methanol ; 90 : 10). After consumption of starting materials, water (100 mL) was added and mixture was extracted into $CHCl_3$. Organic layer was dried on Na_2SO_4 and evaporated. Column chromatographic separation (silica gel, Ethyl acetate : Methanol ; 90 : 10) of the residue yielded the desired product as a green solid. (33 mg, 50%). ^{1}H NMR (400 MHz, $CDCl_3$): δ_H 8.61 (2H, d, *J*

= 5.68 Hz, ArH), 7.67 (2H, t, *J* = 3.89 Hz, ArH), 7.57-7.47 (4H, m: 2H, ArH; 2H, C*H*), 7.46 (2H, d, *J* = 8.80 Hz, ArH), 7.28 (2H, d, *J* = 8.67 Hz, ArH), 7.24-7.15 (3H, m: 2H Ar*H;* 1*H* C*H*), 7.12 (1H, d, *J* = 15.90 Hz, ArH), 7.06 (2H, d, *J* = 8.54, ArH), 6.76-6.70 (4H, m, ArH), 6.65 (2H, d, *J* = 9.00 Hz, ArH), 6.59 (1H, s, Ar*H*), 6.56 (1H, s, Ar*H*), 4.89 (4H, s), 3.85-3.76 (8H, m), 3.72-3.58 (24H, m), 2.92 (4H, t, *J* = 7.92 Hz), 2.76 (4H, t, *J* = 4.94 Hz), 1.52 (6H, s); ^{13}C NMR (100 MHz, $CDCl_3$): δ_C 158.3, 149.8, 149.7, 147.4, 136.9, 135.7, 129.6, 129.3, 129.0, 126.5, 125.3, 122.2, 122.0, 120.9, 112.7, 111.8, 111.5, 74.3, 71.3, 70.7, 70.2, 70.0, 68.6, 57.3, 52.6, 51.9, 38.7, 31.6, 31.3, 30.3, 29.6, 28.9, 15.0, 14.9 ppm. Anal. Calcd. for $C_{65}H_{76}BF_2N_7O_6S_2$: C 67.05, H 6.58, N 8.42 %. Found: C 66.91, H 6.64, N 8.33 %. MS (MALDI-TOF): m/z: Calcd. For $C_{65}H_{76}BF_2N_7O_6S_2$: 1163.5 [$M^+$], Found: 1163.3 [$M^+$].

2.5 UV-Vis Titration Experiments

Titrations of compound **4** with Zn^{2+} ion : 100 μL portions of 0.16 mM stock solution of 4 were diluted to 2 mL by adding acetonitrile (to 3.2 x 10^{-6} M) and to these solutions aliquots of $Zn(Otf)_2$ solutions (0.1 mM) in acetonitrile (0, 160, 320, 480, 640, 800, 960, 1120, 1280, 1600 μL) were added. Volumes of these solutions were adjusted to 5 mL. UV-vis absorption spectra were recorded at room temperature.

Titrations of 4 with Hg(II) ion : 100 μL portions of 0.16 mM stock solution of 4 were diluted to 2 mL by adding acetonitrile (to 3.2 x 10^{-6} M) and to these solutions were added aliquots of $Hg(ClO_4)_2$ solutions (0.1 mM) in acetonitrile (0, 320, 1280, 1440, 1600 μL). Volumes of these solutions were adjusted to 5 mL. UV-vis absorption spectra were recorded at room temperature.

2.6 Isothermal Titration Calorimetry

Isothermal titration Calorimetry (ITC) is used to determine the thermodynamics

of a reaction. The experiments are performed at constant temperature by titrating one binding partner (the titrant) into a solution containing the other partner (the titrand). After each aliquot of titrant is added, the heat absorbed or released by its reaction with the titrand is measured with respect to a reference cell containing buffer. The heat change is measured in electrical power (J/s) as it is the difference in power needed to maintain the sample and reference cells at two similar temperatures. Binding Constant (K_b), Reaction Stoichiometry (n), Heat of Reaction (ΔH) and Entropy of Reaction (ΔS) can be obtained via ITC.

CHAPTER 3

RESULTS & DISCUSSION

3.1 Precise Control of PeT and ICT Processes

Considering their size, reconfigurability and especially bio-integrability, molecular logic devices are promising information processing units. In this research, Bodipy-derived fluorophores have been used to construct an **AND** gate (molecule **2** in Figure 26), a **half-adder** (molecule **4**), and a three-input **AND** gate (molecule **7**). Having remarkable properties such as large extinction coefficient and high quantum yield, Bodipy dyes are widely preferred in chemosensor and molecular logic gate designs. More importantly, recently expanding "Bodipy chemistry" provided facile derivatization possibilities to install PeT and ICT modulators onto the chromophore core.

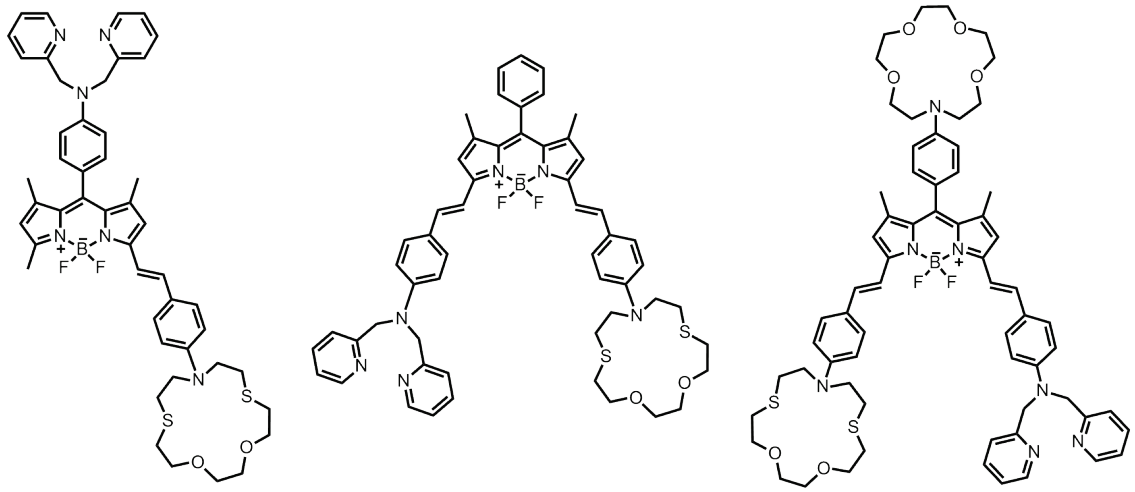

Figure 26. Molecular structures of target logic devices: **AND** gate (2), half-adder (4) and three-input **AND** gate (7) respectively

It is important to note that, *meso*-substituents in these designs are more likely to act as PeT modulators only and their interaction with the ground state is limited. Whereas styrl-tethered receptors directly interact with the ground state and alter HOMO-LUMO levels, since they extend the conjugation of Bodipy core –i.e. they are ICT modulators. PeT donor in molecule **2** and ICT donor in molecules **4** and **7**, the dipicolylamine ligand, is a well-known Zn^{2+} selective ligand. The dithiaazacrown ligand, ICT donor in all three target molecules, is known to have a selectivity for Hg^{2+} over many other metal ions. The azacrown moiety, PeT donor in molecule **7** preferably binds to hard alkaline and alkaline-earth metals, such as Ca^{2+}.

Table 7. Spectral data for target molecules

Compounds	λ_{max} **(nm)**	**Abs (nm)**[a]	ε_{max} **($M^{-1}cm^{-1}$)**	**fwhm (cm^{-1})**	Φ[b]
2	600	0.135	80000	1540	0.1
2 + Zn^{2+}	602	0.132	79000	1640	0.16
2 + Hg^{2+}	560	0.075	53000	2460	0.19
2 + Zn^{2+} + Hg^{2+}	560	0.153	92000	900	0.43
4	697	0.259	81000	1420	0.11
4 + Zn^{2+}	673	0.288	90000	1440	0.33
4 + Hg^{2+}	674	0.294	92000	1640	0.28
4 + Zn^{2+} + Hg^{2+}	630	0.34	106000	840	0.78
5	497	0.101	60600	960	0.012
5 + Ca^{2+}	498	0.095	57000	870	0.592
7	692	0.142	71000	1280	0.038
7 + Ca^{2+} + Zn^{2+} + Hg^{2+}	626	0.122	61000	1240	0.266

[a] Peak absorption values at the specific concentrations of the study.

[b] Quantum yields for compounds 2, 4, and 7 were determined in reference to Sulforhodamine 101 (0.90 in ethanol) and for compound 5 Rhodamine 6G (0.95 in ethanol) was used as a reference.

The spectral data for all three target compounds and their metal complexes were tabulated in Table 7. It is clear that the metal ions separately or together, have different regioselectivities.

3.2 Binding constants

Isothermal titration calorimetry was useful in determining the binding constants of Hg^{2+} and Zn^{2+} (Table 8). Experimentally determined binding affinities confirm the working principle of the proposed molecular logic gates.

Table 8. Binding constants determined by isothermal titration calorimetry (ITC) for the relevant binding events.

Titration	K (M^{-1})	ΔH (kcal/mol)	ΔS cal/(mol.K)	model
Compound **1** (1:1) binding-Zn^{2+}	(4.8 ± 0.4) x 10^7	-7.5 ± 1.6	5.99	two sets of sites
Compound **1** (1:2) binding-Zn^{2+}	(5.9 ± 0.8) x 10^6	-11.4 ± 0.4	-2.95	two sets of sites
Reference[a] dithiaazacrown-Hg^{2+}	(3.4 ± 0.8) x 10^6	-11.6 ± 0.08	-9.27	one set of sites
Compound **1**-Hg+2	(9.1 ± 0.5) x 10^6	-15.3 ± 0.02	-19.3	one set of sites
Half adder **4**-Zn^{2+}	(6.7 ± 0.6) x 10^5	-14.9 ± 0.1	-23.2	one set of sites
Half adder **4**-Hg^{2+}	(8.0 ± 2.6) x 10^7	-39.4 ± 0.3	-95.6	two sets of sites
Half adder **4**-Hg^{2+} 2nd binding	(1.1 ± 0.2) x 10^5	-1.1 ± 0.2	-41.1	two sets of sites
AND Gate **2**-Zn^{2+}	(1.8 ± 0.8) x 10^6	-6.8 ± 0.2	5.7	one set of sites
AND Gate **2**-Hg^{2+}	(1.3 ± 0.9) x 10^8	-12.0 ± 0.1	-3.18	two sets of sites
AND Gate **2**-Hg^{2+} 2nd binding	(7.7 ± 1.2) x 10^4	-8.1 ± 0.2	-4.74	two sets of sites

[a] The reference compound used here is N-(4-formylphenyl)-1-aza-4,13-dithia-[15]crown-5.

At high concentrations of compound **1** (Figure 27)**,** a clear 1:2 complexation is observed**.** Similar interaction is not observed when the dipicolylamine ligand is tethered with a styryl group to 3 (or 5) position of Bodipy, which can be understood in terms of steric demands of 1:2 interaction.

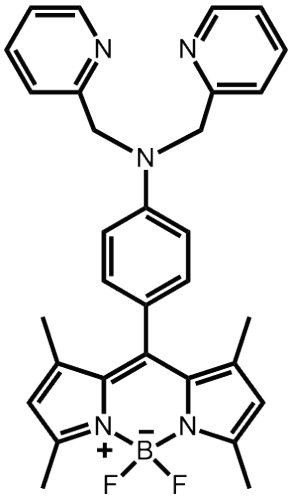

Figure 27. Molecule **1** is used as a reference in ITC experiments

Half-adder molecule **4** (0.4 mM) when titrated with 5.0 mM Zn^{2+} ions shows just one binding, indicating an affinity for the picolylamine ligand, but not for the dithiaazacrown ligand (Figure 28). The two-input **AND** logic titration with Zn^{2+} ions also shows just one binding event. Compared to that of Hg^{2+} ions, larger affinity of Zn^{2+} ions for dipicolylamine ligand apparent in the separate titration studies (Figure 29) done with these two cations and the reference compound **1 (**4.8 x 10^7 M^{-1} for Zn^{2+} and 9.1 x 10^6 M^{-1} for Hg^{2+}).

Titration of ditopic compounds with Hg^{2+} ions revealed that, Hg^{2+} have strong affinities for both dipicolylamine and the dithiaazacrown ligands, and at larger concentrations both ligands would be engaged. But at the selected concentrations of Zn^{2+} and Hg^{2+} as inputs, dynamic nature of the binding events dictate that Zn^{2+} ions with no affinity to dithiaazacrown ligand and larger affinity for dipicolyl

ligand will preferentially occupy dipicolylamine ligand. This order of affinity will be in place for all three logic gates designs.

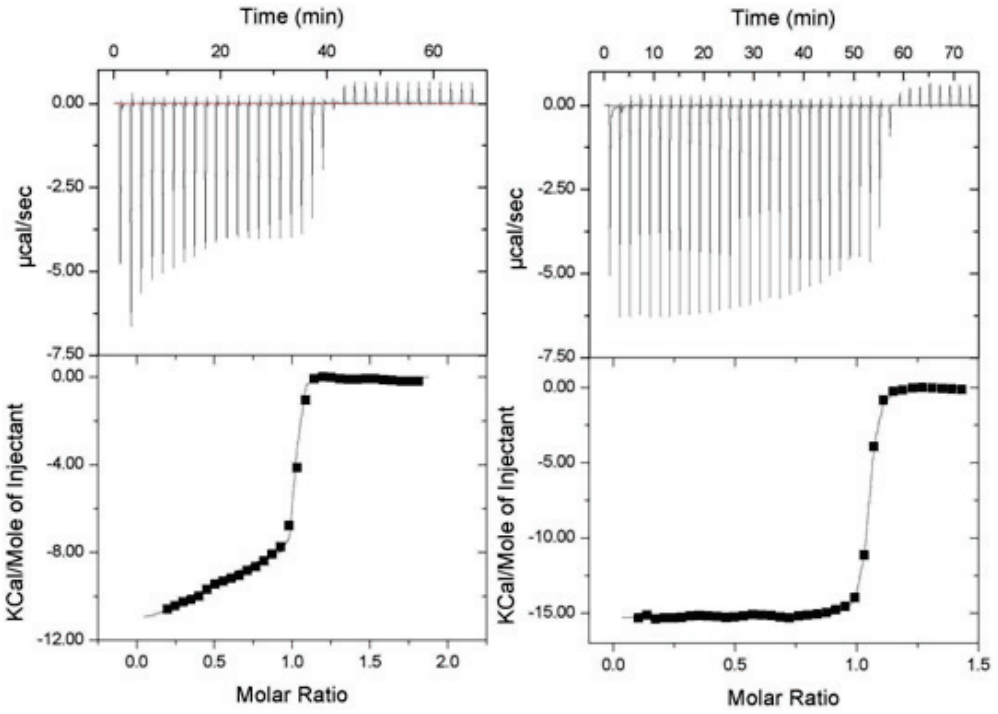

Figure 28. ITC titration curves of compound **4** in acetonitrile

On the other hand, binding affinity of Ca^{2+} ions were significantly smaller, therefore relavant binding constant in the interaction of these ions with three-input logic gate molecule **7** were determined by spectrofluorometry. The value obtained for K is 680 M^{-1} (Figure 30) suggests that at higher input concentrations of Ca^{2+} ions, the crown ether moiety will be engaged by this cation.

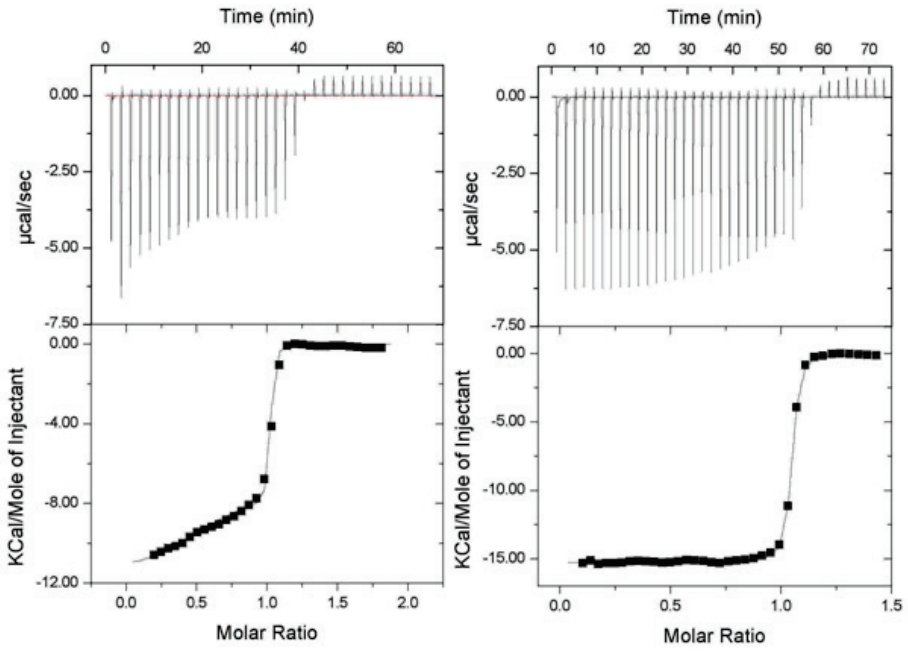

Figure 29. ITC titration curves of reference compound **1** in acetonitrile

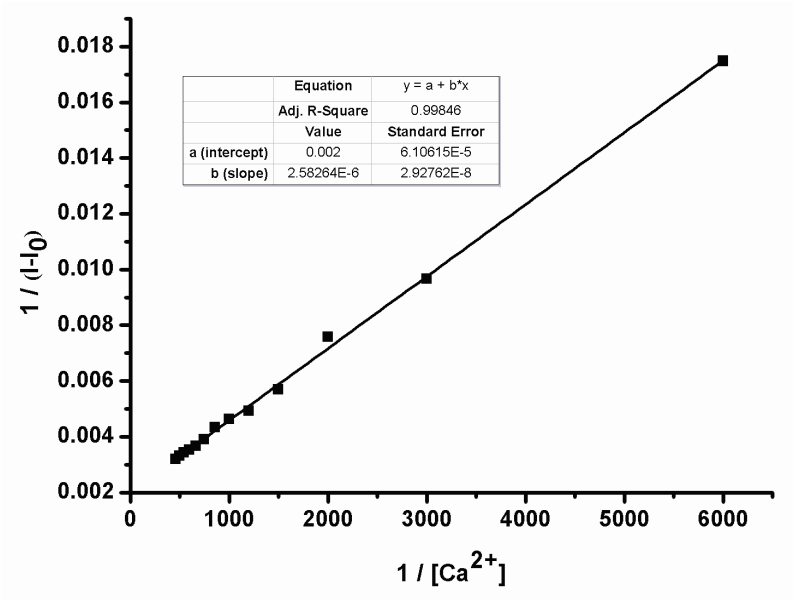

Figure 30. Benesi-Hildebrand analysis of fluorimetric Ca^{2+} titration data for compound **5**.

3.3 AND Gate

Figure 31 shows the emission spectra of molecule **2** upon addition of the metal cation modulators. In the absence of cations, dye emission spectrum has a broad peak, with a maximum at 679 nm.

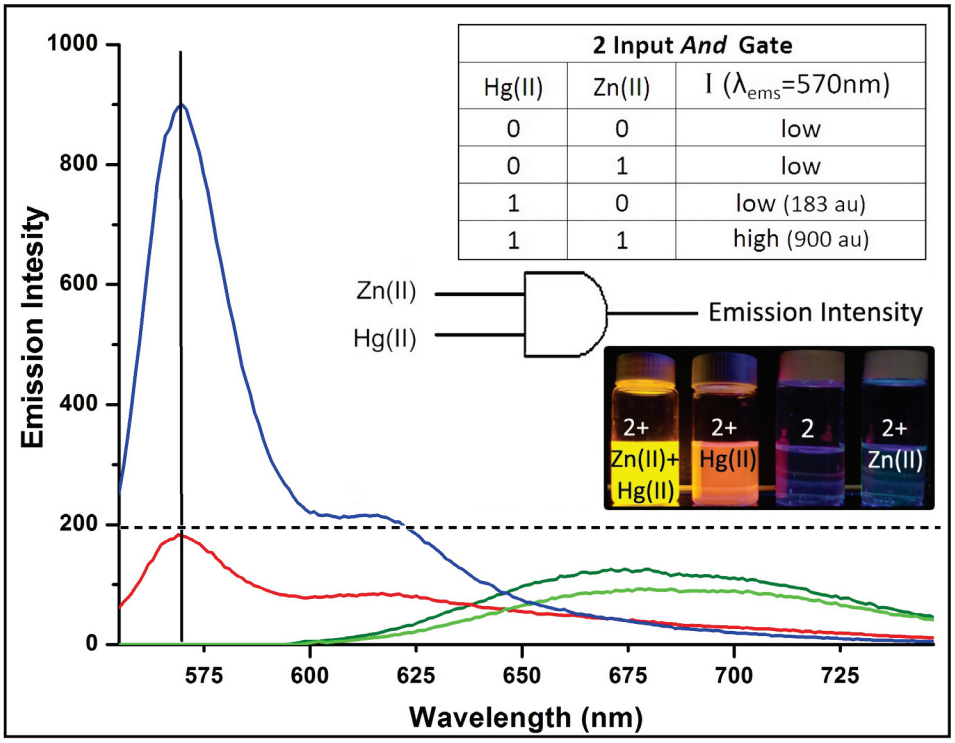

Figure 31. Fluorescence emission of molecule **2** exhibits **AND** gate behavior

When Zn^{2+} was cation is added, as perchlorate salt, very small changes in the emission spectrum observed: peak intensity increased slightly, while peak maximum did not change. This observation can be rationalized considering the fact that in the longer wavelength region of the spectrum *(vide infra)* PeT process is usually not significant due to large number of vibrational relaxation pathways. Hence, the effect of Zn^{2+} cation addition, which selectively binds to PeT donor dipicolylamine moiety at *meso* position at the applied concentration (1.67 μM),

rather than the ICT donor dialkylaminophenyl group in full conjugation with the Bodipy core stays minimal.

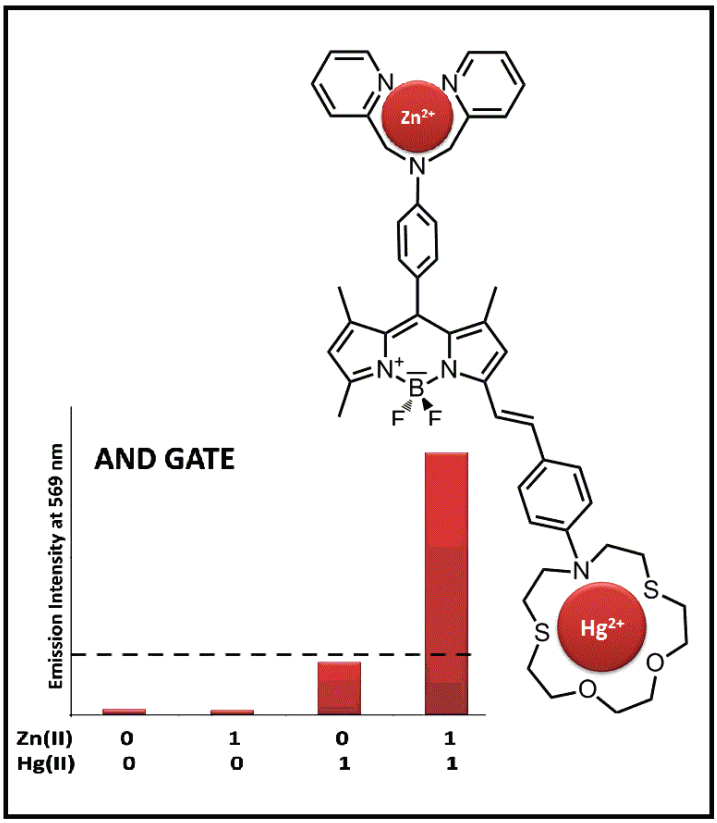

Figure 32. Emission intensities at 596 nm shown in bar-graphed truth table

Whereas Hg^{2+} addition (6.68μm) alters the spectrum significantly. Soft Hg^{2+} cations selectively binds to ICT donor thiaazacrown ligand which results a blue shift of 109 nm. As explained in Section 1.2.4, reduced charge transfer upon metal cation binding causes an increase in the HOMO-LUMO gap. When hypsochromic shift occurs, however, PeT process become activated and emission intensity (570 nm peak) stays low.

Thereby, only in the presence of both Hg^{2+} and Zn^{2+} cations, PeT donating ability of the dipicolyamine substituent is blocked and an intense emission peak at 570 nm is

observed. Figure 28 shows the colorful signaling which is in accordance with the **AND** logic when the emission is recorded at 570 nm.

A theoretical model for molecule **2** has also been studied at DFT B3LYP/6-31G level. As a reasonable model for cation binding, protonation of donor nitrogen atoms in the PeT and ICT active groups is used. Calculations revealed changes in the frontier orbitals (shown in Figure 33) that supports the above explanation.

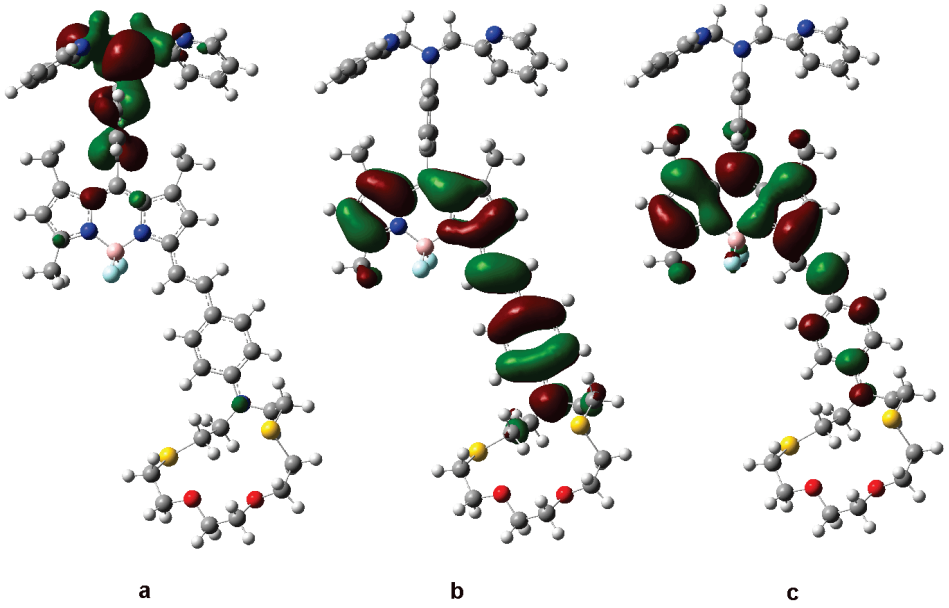

Figure 33. Frontier orbitals for molecule **2** (a:HOMO-1, b:HOMO, c:LUMO)

Table 9 shows the calculated energies of frontier orbitals. Relative changes of energy values are also shown schematically in Figure 34 with LUMO levels aligned for clarity. Following can be said relying on these calculations: i- The major transition is always from the dye centered (DC in Figure 34) orbital (HOMO or HOMO-1) to the LUMO, which is again invariably dye centered. ii-PeT activity is linked to the presence of a ligand centered HOMO (here ligand refers specifically to the dipicolylamine ligand) above a dye-centered orbital, to the energy gap between

this HOMO orbital and the dye-centered HOMO-1. The magnitude of this gap is related to the thermodynamic driving force for PeT and thus the rate of PeT.

Table 9. Energies of the frontier orbitals (LC-stands for ligand centered, DC for dye-centered)

	Occupied		Unoccupied
Dyes	LC (eV)	DC (eV)	LUMO (eV)
2	-5.31	-4.46	-2.29
2 + H^+ [Hg(II)]	-6.64	-7.24	-4.73
2 + H^+ [Zn(II)]	-9.74	-6.15	-4.24
2 + $2H^+$ [Zn(II) + Hg(II)]	-11.7	-9.09	-6.69

In the absence of both cations, since HOMO is dye centered, PeT pathway is blocked. Still, only a low-intensity emission is present, due to the larger number of non-radiative decay pathways at longer wavelength transitions.

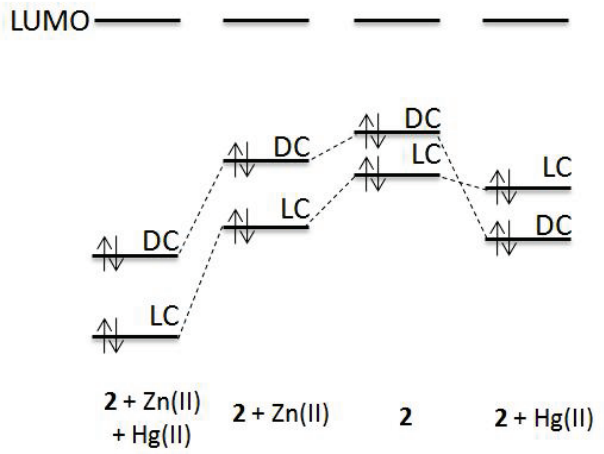

Figure 34. Changes in the energy levels of the frontier orbitals (LUMO levels aligned for clarity)

Calculations show that Hg^{2+} addition effects DC occupied orbital largely while LC occupied orbital is only slightly effected. This result is important for two reasons: i- Hg^{2+} addition increases HOMO-LUMO gap largely, that accounts for 109 nm of blue shift, ii- Order of the occupied orbitals in terms of their energy is changed after Hg^{2+} addition, which activated the dipicolylamine group as a PeT donor. This is why, when Hg^{2+} ions were added, there is a blue shift, but no increase in the emission intensity. In 1:1 complex of **2**-Hg^{2+}, PeT is expected to be more effective.

In the case that only Zn^{2+} cations were added, energetic order of frontier orbitals are not changed but their relative positions are affected slightly. Since PeT donor is not in conjugation with the Bodipy core, dye-centered orbitals are affected less when compared to ligand-centered orbitals. This actually translates as little or no change in the emission character as the HOMO-LUMO gap is moderately affected.

But when both cations were added, a significant increase in the HOMO-LUMO gap due to reduced charge transfer (blue shift for the main transition), and large stabilization of the ligand-centered (dipicolyamine) orbitals (blocking of PeT) were in effect. The net result is a blue-shifted intense emission.

3.4 Half-adder in the Absorption Mode

In half-adder molecule **4**, both two receptors are in full conjugation with the Bodipy core and they function as ICT donors. The spectral changes are direct consequences of relative affinities of these ligands to Hg^{2+} cations[99] and Zn^{2+} cations[100].

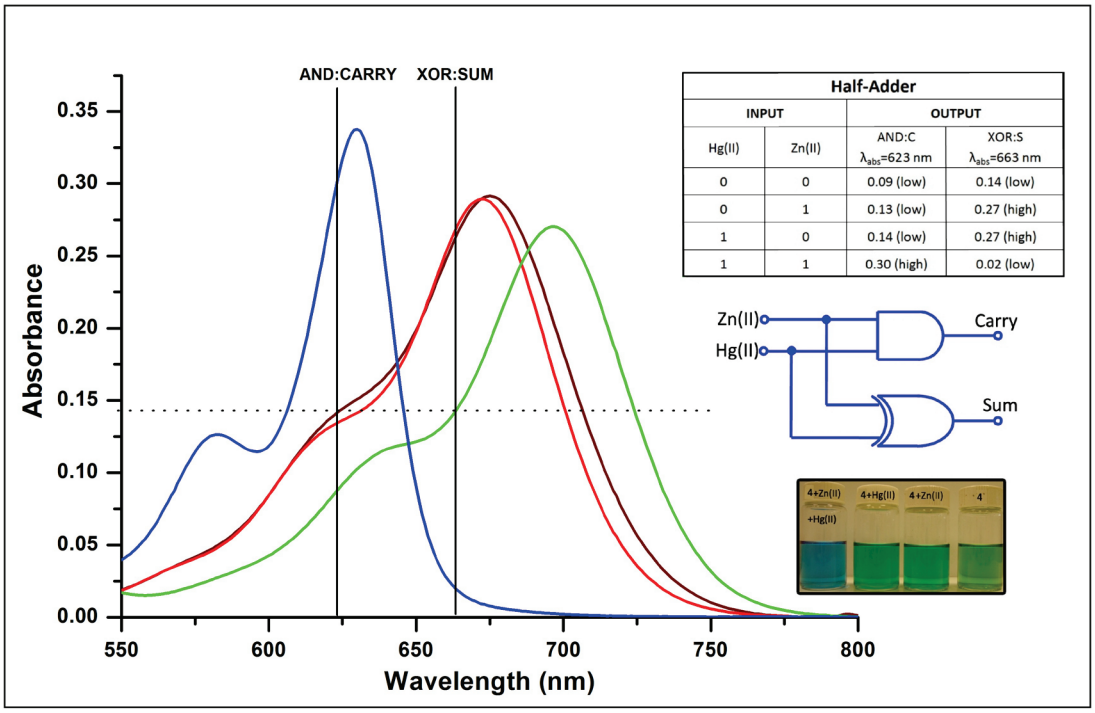

Figure 35. Absorbance spectra for molecule **4** in the absence and presence of analytes

Distyryl-Bodipy dye **4** alone has an absorption peak with a peak maximum at 698 nm (Figure 35). Upon Zn^{2+} addition, since charge transfer from dipicolylamine ligand is blocked, a small blue shift to 675 nm observed. Similar results are obtained when only Hg^{2+} cations are added to the solution, since mercuric cations block charge transfer caused by dithiaazacrown ligand only. Clearly, even in the excess of these cations, ICT is blocked partially due to high selectivity of both ligands.

However, in the presence of both Zn^{2+} and Hg^{2+} cations, the peak shifts further towards shorter wavelengths and peak maximum locates at 630 nm. Hence absorption spectrum contains intense peaks at around 675 nm only if one of the cations is present, but not both, i.e. molecule exhibits **XOR** gate characteristic around 675 nm. Also absorption signal at around 630 nm translates as an **AND**

gate, since neither dye **4** alone, nor its complex with one of the cations absorb at that short wavelength. Since these two gates are operated in parallel, molecule reads as a half-adder. The truth tables for the two logic gates are shown graphically in Figure 36, monitored at fine-tuned wavelengths (623 nm for **AND** gate, 663 nm for **XOR)**.

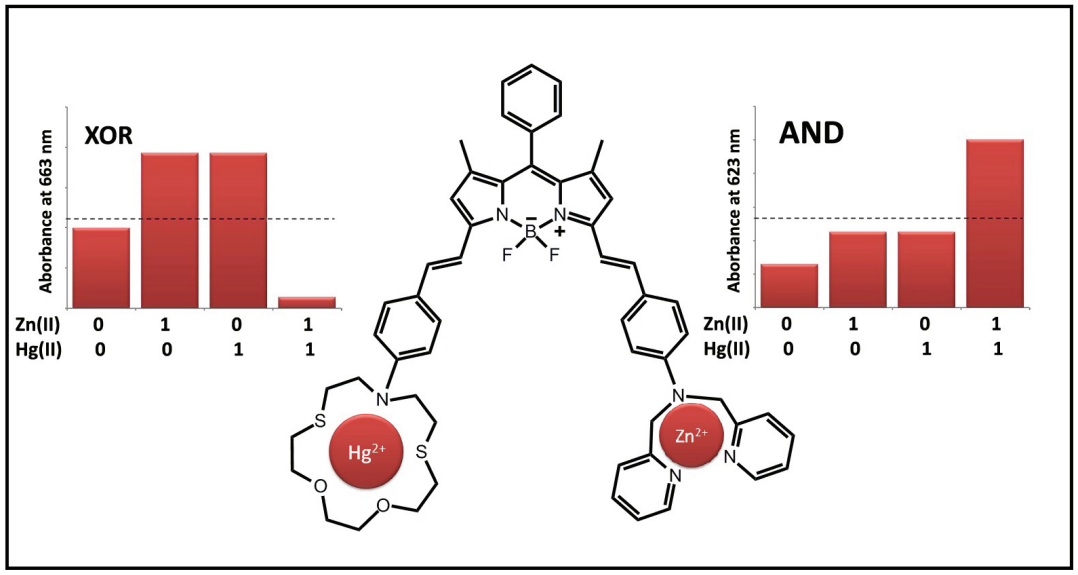

Figure 36. Absorbance intensities at 663 and 623 nm shown in bar-graphed truth table

3.5 A three-input AND Gate

Absorption spectrum of the ternucleating (tritopic) compound **7** is presented in Figure 37, and the effects of added metal ions (Ca^{2+}, Zn^{2+} and Hg^{2+}) are apparent. Harder Ca^{2+} ions prefer to interact with harder azacrown ligand at the *meso* position of the Bodipy dye. This interaction is not expected to alter the absorption spectrum, but since it has to be added at a larger concentration (1.0 mM) than the other metal ions, a minor 25 nm blue shift is nevertheless observed, indicating some interference at the ICT donor ligands.

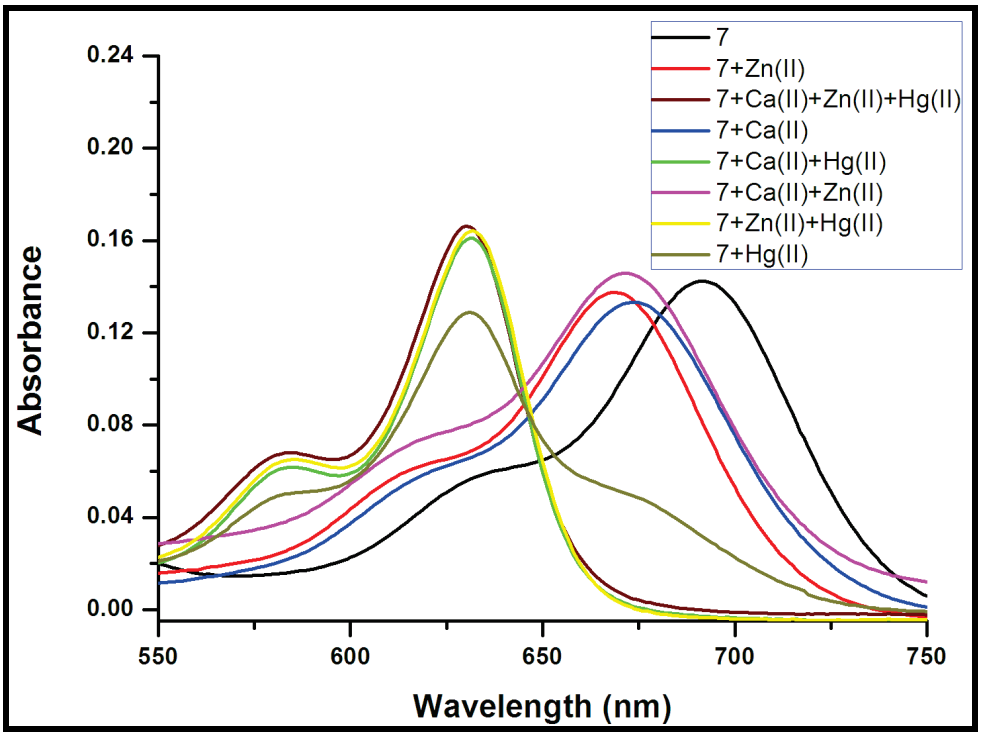

Figure 37. Absorption spectrum for molecule **7**

When compared to free fluoroionophore, approximately 25 nm blue shift was observed in the absorption spectra for the following combinations: Ca^{2+}, Zn^{2+} and Ca^{2+}+Zn^{2+}. Hg^{2+} is particularly effective, and in all input scenarios including Hg(II), there is large 70 nm hypsochromic shift. Nevertheless, it is obvious that absorbance changes seem far too complicated to be of much use in logic gate design. However, the emission changes (Figure 38) result in a better picture for this purpose. At the concentrations used in the present work (Hg^{2+} and Zn^{2+} at 20.0 μM and Ca^{2+} at 1.0 mM), only when all three cations were added as inputs, emission is significantly enhanced above the threshold. The three cations separately, or in other binary combinations, do not induce an enhanced and blue shifted emission from the compound **7**. Thus, all three metal cation inputs are required simultaneously for the large emission increase at 656 nm, this behavior is in accordance with an **AND** logic gate.

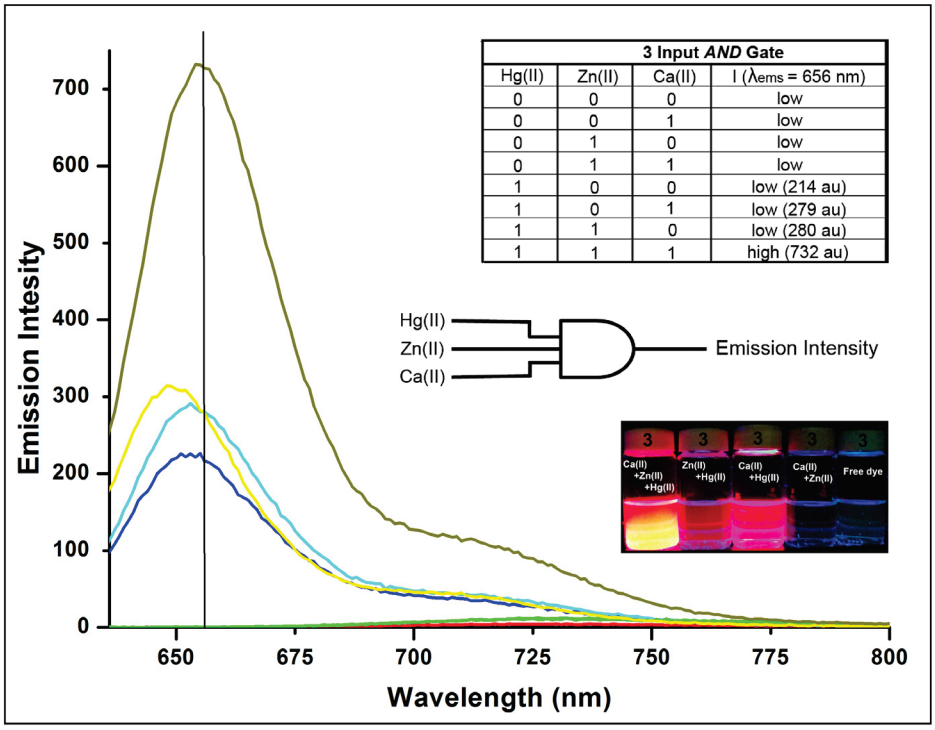

Figure 38. Fluorescence emission of molecule 7 exhibits a three-input **AND** gate characteristics

One can envision a scenario, where elevated concentrations of three different molecular or ionic species may indicate a particular disease state (lab-on-a molecule, as elaborated previously by de Silva), thus a non-zero **AND** logic response, could be a positive identification of that particular state. The use of multiple photophysical processes for eliciting an **AND** response is highly relevant, as it would minimize false positives, since for example in this case, both a blue shift and large enhancement of emission signal should be expected. In addition, simultaneous sensing is also possible: PeT and ICT processes can clearly be addressed separately, for shorter wavelength emitting fluorophores PeT processes can be effective, and be separately blocked by an appropriate metal ion, resulting signal enhancement, regardless of the ICT modulating ions. On the other hand, ICT

donor ligand will result in spectral shift which can be correlated to the concentration of the analyte targeting that particular ligand.

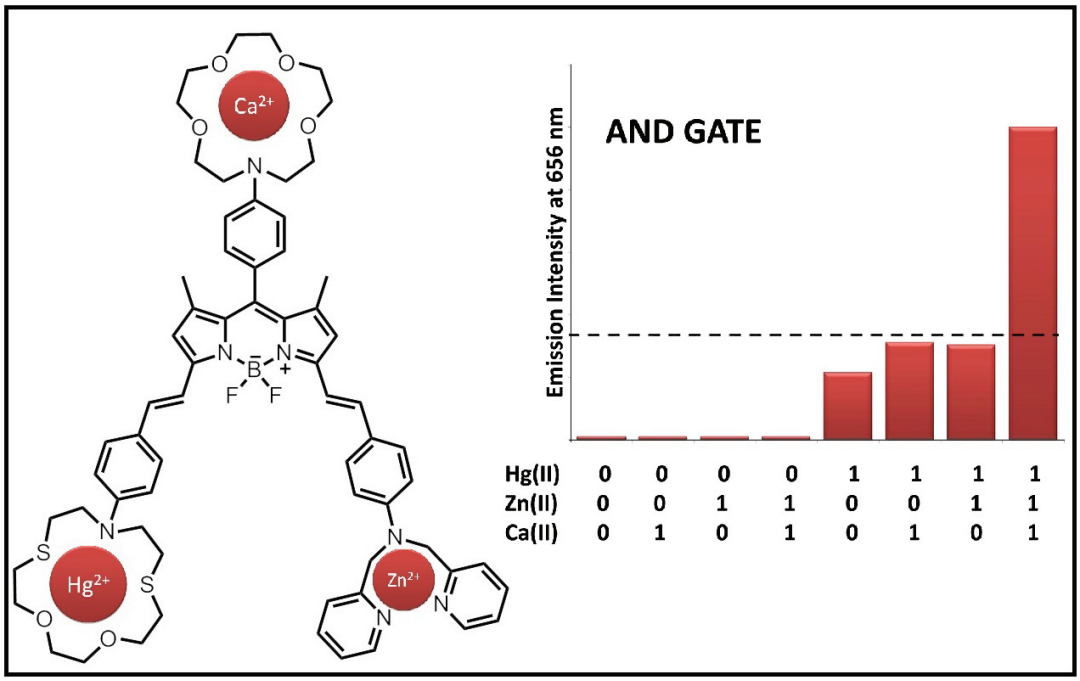

Figure 39. Emission intensities at 656 nm shown in a bar-graphed truth table

CHAPTER 4

CONCLUSION

We demonstrated that with a prior knowledge of respective binding affinities of metal ions for various ligands, it should be possible to design molecular logic gates using different metal ions as inputs. Remarkably versatile chemistry of Bodipy is particularly useful in this regard, because it allows straightforward placement of ICT and PeT donors on the same molecule, and this increases signal diversity to a great extent. Styryl-modifications of Bodipy proved to be a useful reaction. In the three examples presented, this modification allowed us to place ICT donor functionalities at strategically important positions. The result is straightforward syntheses of the target molecules, with responses compatible with **AND** logic and, a molecular half-adder with non-annihilating inputs. Outputs compatible with **XOR** logic has been difficult to attain without the use of self-annihilating (such as acids and bases, either Lewis or Bronsted-Lowry) inputs, but in the half-adder described in this work, this is done by the differential selective interactions between the ligands and the metal ions selected. The results suggest that different metal ions can be used as non-annihilating inputs, selectively targeting various ligands incorporated within a single fluorophore, and with careful design, diverse photophysical processes can be selectively modulated, resulting in a range of signals, useful in molecular logic design, and offering an enticing potential for multianalyte chemosensors Using signals obtained by exploiting relative selectivity of inputs for different ligands/chelators, more challenging molecular logic operations should be within reach.

REFERENCES

1. C.J. Pedersen, *J. Am. Chem. Soc* **89**, 7017-7036, 1967.
2. J.F. Stoddart, *Nature Chemistry* **1**, 14–15, 2009.
3. J.M. Lehn, *Angew. Chem. Int. Ed.* **27**,, 1988.
4. E.U. Akkaya, S. Ozlem, *J. Am. Chem. Soc* **131**, 48-49, 2009.
5. D. Shabat, R.J. Amir, M. Popkov, R.A. Lerner, C.F. Barbas, *Angew. Chem. Int. Ed.* **44**, 4378-4381, 2005.
6. J.L. Atwood, J.W. Steed, *Encyclopedia of Supramolecular Chemistry* (CRC Press: 2004).
7. *Philosophical Magazine* (Taylor & Francis.: 1854).
8. P. Siffert, E.F. Krimmel, *Silicon* (Springer: 2004).
9. *Computer, "n."* (Oxford University Press: 1989).
10. *Approximate Desktop, Notebook, & Netbook Power Usage* at http://www.upenn.edu/computing/provider/docs/hardware/powerusage.html [accessed 17 May 2010]
11. *Replica of First Transistor (JPEG Image)* at http://clinton4.nara.gov/media/jpg/replica-of-first-transistor.jpg [accessed 17 May 2010]
12. *Nano-Transistor (JPEG Image)* at http://www.nanopicoftheday.org/images/nanotransistor.jpg [accessed 17 May 2010]
13. G.E. Moore, *Proc. IEEE.* **86**, 82–85, 1998.
14. M. Kanellos, *New Life for Moore's Law*, *CNET News* at http://news.cnet.com/New-life-for-Moores-Law/2009-1006_3-5672485.html [accessed 17 May 2010]
15. *Moore Law Diagram (JPEG Grafiği)* at http://upload.wikimedia.org/wikipedia/commons/a/a9/Moore_Law_diagram_%282004%29.jpg [accessed 1 July 2010]

16. R.P. Feynman, *J. Microel. Sys.* **1**, 60–66, 1992.
17. P.A. de Silva, N.H.Q. Gunaratne, C.P. McCoy, *Nature* **364**, 42-44, 1993.
18. G.G. Stokes, *Org. Lett.* **142**, 463-562, 1852.
19. J.R. Lakowicz, *Principles of Fluorescence Spectroscopy* (Springer: 2006).
20. M. Wasielewski, J. Fenton, Govindjee, Govindjee, *Photosyn. Res.* **12**, 181-189, 1987.
21. A.W. Czarnik, A.C.S.D.O.O. Chemistry, A.C.S. Meeting, *Fluorescent Chemosensors for Ion and Molecule Recognition* (American Chemical Society: 1993).
22. T. Nagano, T. Matsumoto, Y. Urano, T. Shoda, H. Kojima, *Org. Lett.* **9**, 3375-3377, 2007.
23. E.U. Akkaya, C.N. Baki, *J. Org. Chem* **66**, 1512-1513, 2001.
24. L. Fabbrizzi, A. Poggi, *Chem. Soc. Rev.* **24**, 197-202, 1995.
25. A.P. de Silva, R. Bissell, H. Nimal Gunaratne, P. Mark Lynch, G. Maguire, C. McCoy, K. Samankumara Sandanayake, *Photoinduced Electron Transfer V* 223-264, 1993.
26. E. Van der Donckt, *Prog. React. Kinet* **5**, 273, 1970.
27. B. Valeur, M.M. Martin, P. Plaza, Y.H. Meyer, L. Bégin, J. Bourson, *J. Fluor.* **4**, 271-273, 1994.
28. B. Valeur, M. Martin, P. Plaza, N. Dai Hung, Y. Meyer, J. Bourson, *Chem. Phys. Lett.* **202**, 425-430, 1993.
29. B. Valeur, M.M. Martin, P. Plaza, Y.H. Meyer, F. Badaoui, J. Bourson, J. Lefevre, *J. Phys. Chem* **100**, 6879-6888, 1996.
30. E.U. Akkaya, E. Deniz, G.C. Isbasar, O.A. Bozdemir, L.T. Yildirim, A. Siemiarczuk, *Org. Lett* **10**, 3401-3403, 2008.
31. E.U. Akkaya, H.T. Baytekin, *Org. Lett.* **2**, 1725-1727, 2000.
32. A. Shanzer, D. Margulies, G. Melman, C.E. Felder, R. Arad-Yellin, *J. Am. Chem. Soc* **126**, 15400-15401, 2004.
33. A.P. de Silva, S. Uchiyama, *Nat. Nano* **2**, 399-410, 2007.

34. K. Szaciłowski, *Chem. Rev.* **108**, 3481-3548, 2008.
35. A.P. de Silva, N.D. McClenaghan, *Chem. A. Eur. J.* **10**, 574-586, 2004.
36. V. Balzani, A. Credi, M. Venturi, *Chem. Phys. Chem.* **4**, 49-59, 2003.
37. S.J.M. Koskela, T.M. Fyles, T.D. James, *Chem. Commun. (Camb.)* 945-947, 2005. [doi:10.1039/b415522j]
38. S. Shinkai, T.D. James, K.R.A.S. Sandanayake, *Angew. Chem. Int. Ed.* **33**, 2207-2209, 1994.
39. D. Zhu, G. Zhang, D. Zhang, Y. Zhou, *J. Org. Chem* **71**, 3970-3972, 2006.
40. A.P. de Silva, D.C. Magri, G.J. Brown, G.D. McClean, *J. Am. Chem. Soc* **128**, 4950-4951, 2006.
41. M.D. Lankshear, A.R. Cowley, P.D. Beer, *Chem. Commun.* 612-614, 2006.
42. A.P. de Silva, K.R.A.S. Sandanayake, *Angewandte Chemie International Edition in English* **29**, 1173-1175, 1990.
43. A.P. de Silva, S. Uchiyama, K. Iwai, G.D. McClean, *J. Am. Chem. Soc* **127**, 8920-8921, 2005.
44. A.P. de Silva, H.Q.N. Gunaratne, C.P. McCoy, *J. Am. Chem. Soc* **119**, 7891-7892, 1997.
45. A.P. de Silva, J.F. Callan, N.D. McClenaghan, *Chem. Commun. (Camb.)* 2048-2049, 2004. [doi:10.1039/b405909c]
46. H. Wang, D. Zhang, X. Guo, L. Zhu, Z. Shuai, D. Zhu, *Chem. Commun. (Camb.)* 670-671, 2004. [doi:10.1039/b312360j]
47. A. de Silva, H. GUNARATNE, G. MAGUIRE, *J. Chem. Soc. - Chem. Comm.* 1213-1214, 1994.
48. U. Pischel, M. de Sousa, M. Kluciar, S. Abad, M.A. Miranda, B. de Castro, *Photochem. Photobiol. Sci.* **3**, 639, 2004.
49. H. Miyaji, S.R. Collinson, I. Prokeŝ, J.H.R. Tucker, *Chem. Commun. (Camb.)* 64-65, 2003.
50. J. Montenegro, E. Perez-Inestrosa, D. Collado, Y. Vida, R. Suau, *Org. Lett* **6**, 2353-2355, 2004.

51. M.S. Park, K. Swamy, Y.J. Lee, H.N. Lee, Y.J. Jang, Y.H. Moon, J. Yoon, *Tetrahedron Letters* **47**, 8129-8132, 2006.
52. T. Hirai, G. Nishimura, K. Ishizumi, Y. Shiraishi, *J Phys Chem B* **110**, 21596-21602, 2006.
53. H. Miyaji, H. Kim, E. Sim, C. Lee, W. Cho, J.L. Sessler, C. Lee, *J. Am. Chem. Soc.* **127**, 12510-12512, 2005.
54. A.P. de Silva, I.M. Dixon, H.Q.N. Gunaratne, T. Gunnlaugsson, P.R.S. Maxwell, T.E. Rice, *J. Am. Chem. Soc.* **121**, 1393-1394, 1999.
55. D. Parker, T. Gunnlaugsson, D.A. Mac Dónaill, *J. Am. Chem. Soc* **123**, 12866-12876, 2001.
56. D. Zhu, Y. Li, H. Zheng, Y. Li, S. Wang, Z. Wu, P. Liu, Z. Gao, H. Liu, *J. Org. Chem* **72**, 2878-2885, 2007.
57. F. Vögtle, G. Bergamini, C. Saudan, P. Ceroni, M. Maestri, V. Balzani, M. Gorka, S. Lee, J. van Heyst, *J. Am. Chem. Soc* **126**, 16466-16471, 2004.
58. M. Ward, *Coord. Chem. Rev.* **250**, 3128-3141, 2006.
59. P. de Silva, K.C. Loo, B. Amorelli, S.L. Pathirana, M. Nyakirang'ani, M. Dharmasena, S. Demarais, B. Dorcley, P. Pullay, Y.A. Salih, *J. Mater. Chem.* **15**, 2791, 2005.
60. A.P. de Silva, H.Q.N. Gunaratne, C.P. McCoy, *Chem. Commun.* 2399, 1996. [doi:10.1039/cc9960002399]
61. A. Credi, V. Balzani, S.J. Langford, J.F. Stoddart, *J. Am. Chem. Soc.* **119**, 2679-2681, 1997.
62. F. Gao, H. Chao, F. Zhou, B. Peng, L. Ji, *Inorg. Chem. Comm.* **10**, 170-173, 2007.
63. M. Han, L. Gao, Y. Lü, K. Wang, *J Phys Chem B* **110**, 2364-2371, 2006.
64. A.P. de Silva, N.D. McClenaghan, *Chemistry - A European Journal* **8**, 4935-4945, 2002.
65. D. Qu, Q. Wang, H. Tian, *Angew. Chem. Int. Ed.* **44**, 5296-5299, 2005.
66. D. Zhu, Y. Zhou, H. Wu, L. Qu, D. Zhang, *J. Phys. Chem. B* **110**, 15676-

15679, 2006.

67. D. Gust, J. Andréasson, S.D. Straight, G. Kodis, C. Park, M. Hambourger, M. Gervaldo, B. Albinsson, T.A. Moore, A.L. Moore, *J. Am. Chem. Soc.* **128**, 16259-16265, 2006.
68. A. Shanzer, D. Margulies, G. Melman, C.E. Felder, R. Arad-Yellin, *J. Am. Chem. Soc.* **126**, 15400-15401, 2004.
69. E.K.L. Yeow, R.P. Steer, *Phys. Chem. Chem. Phys.* **5**, 97-105, 2003.
70. A.P. de Silva, G.J. Brown, S. Pagliari, *Chem. Commun.* 2461-2464, 2002. [doi:10.1039/b207795g]
71. R.D. Levine, F. Remacle, R. Weinkauf, *J. Phys. Chem. A* **110**, 177-184, 2006.
72. D. Zhu, X. Guo, D. Zhang, G. Zhang, *J. Phys. Chem. B* **108**, 11942-11945, 2004.
73. D. Gust, J. Andréasson, G. Kodis, Y. Terazono, P.A. Liddell, S. Bandyopadhyay, R.H. Mitchell, T.A. Moore, A.L. Moore, *J. Am. Chem. Soc.* **126**, 15926-15927, 2004.
74. A.P. de Silva, N.D. McClenaghan, *J. Am. Chem. Soc.* **122**, 3965-3966, 2000.
75. A. Shanzer, D. Margulies, G. Melman, *Nat. Mater.* **4**, 768-771, 2005.
76. S.J. Langford, T. Yann, *J. Am. Chem. Soc* **125**, 11198-11199, 2003.
77. E. Perez-Inestrosa, J. Montenegro, D. Collado, R. Suau, J. Casado, *J Phys Chem B* **111**, 6904-6909, 2007.
78. M. Suresh, A. Ghosh, A. Das, *Tetrahedron Letters* **48**, 8205-8208, 2007.
79. W. Sun, Y. Zheng, C. Xu, C. Fang, C. Yan, *J. Phys. Chem. C* **111**, 11706-11711, 2007.
80. E.U. Akkaya, A. Coskun, E. Deniz, *Org. Lett* **7**, 5187-5189, 2005.
81. M. Suresh, D.A. Jose, A. Das, *Org. Lett* **9**, 441-444, 2007.
82. M. Levine, *Proc. Nat. Ac. Sci.* **98**, 9842-9846, 2001.
83. F. Remacle, *Chem. Phys.* **281**, 363-372, 2002.
84. Y. Liu, W. Jiang, H. Zhang, C. Li, *J Phys Chem B* **110**, 14231-14235, 2006.
85. A. Shanzer, D. Margulies, G. Melman, *J. Am. Chem. Soc* **128**, 4865-4871,

2006.

86. A. Shanzer, D. Margulies, C.E. Felder, G. Melman, *J. Am. Chem. Soc.* **129**, 347-354, 2007.
87. D. Gust, J. Andréasson, S. Straight, S. Bandyopadhyay, R. Mitchell, T. Moore, A. Moore, *Angew. Chem. Int. Ed.* **46**, 958-961, 2007.
88. D. Gust, J. Andreasson, S. Straight, S. Bandyopadhyay, R. Mitchell, T. Moore, A. Moore, *J. Phys. Chem. C* **111**, 14274-14278, 2007.
89. M. Irie, *Chem. Rev.* **100**, 1685-1716, 2000.
90. F. Würthner, M. Berberich, A. Krause, M. Orlandi, F. Scandola, *Angew. Chem. Int. Ed.* **47**, 6616-6619, 2008.
91. U. Pischel, *Angew. Chem. Int. Ed.* **46**, 4026-4040, 2007.
92. U. Pischel, *Aust. J. Chem.* **63**, 148-164, 2010.
93. U. Pischel, J. Andreasson, *Chem. Soc. Rev.* **39**, 174-188, 2010.
94. A.P. de Silva, D.C. Magri, G.J. Brown, G.D. McClean, *J. Am. Chem. Soc.* **128**, 4950-4951, 2006.
95. X. Peng, J. Du, J. Fan, J. Wang, Y. Wu, J. Zhao, S. Sun, T. Xu, *J. Am. Chem. Soc* **129**, 1500-1501, 2007.
96. J. Ishikawa, H. Sakamoto, T. Mizuno, M. Otomo, *Bull. Chem. Soc. Jpn.* **68**, 3071-3076, 1995.
97. D.C. Magri, G.J. Brown, G.D. McClean, A.P. de Silva, *Journal of the American Chemical Society* **128**, 4950-4951, 2006.
98. M. Vladimirova, *Dyes and Pigments* **50**, 157-162, 2001.
99. M. Yuan, Y. Li, J. Li, C. Li, X. Liu, J. Lv, J. Xu, H. Liu, S. Wang, D. Zhu, *Org. Lett.* **9**, 2313-2316, 2007.
100. S. Atilgan, T. Ozdemir, E.U. Akkaya, *Org. Lett.* **10**, 4065-4067, 2008.

APPENDIX A

ADDITIONAL UV-VIS DATA

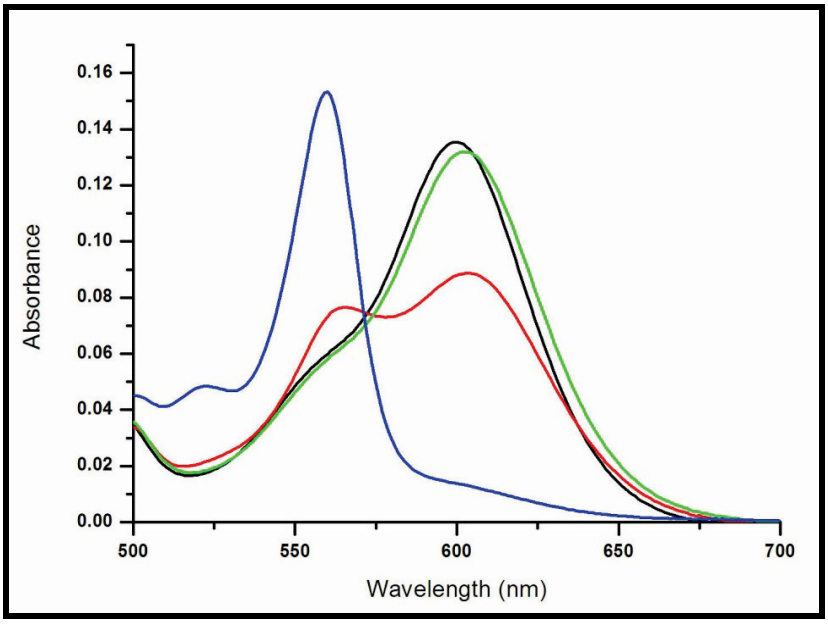

Figure 40. Absorption spectra of **2** (1.67 μM) in acetonitrile in the presence of Hg(II) and Zn(II) (6.68 μM and 1.67 μM, respectively). Green, Zn(II); black no metal ions; red, Hg(II); blue, (Hg(II) and Zn(II).

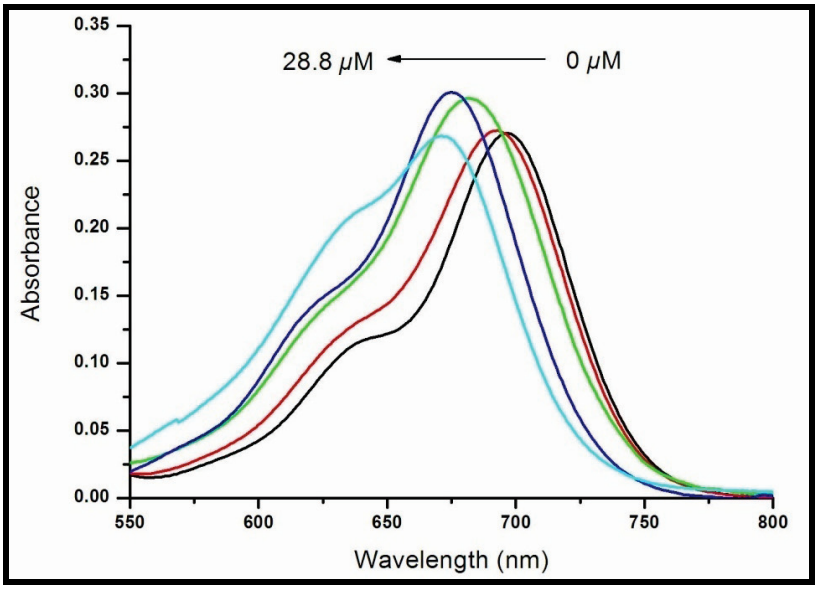

Figure 41. Absorbance spectra of compound **4** in acetonitrile in the presence of increasing Hg(II) concentrations (0, 6.4, 25.6, 28.8, 32.0 μM).

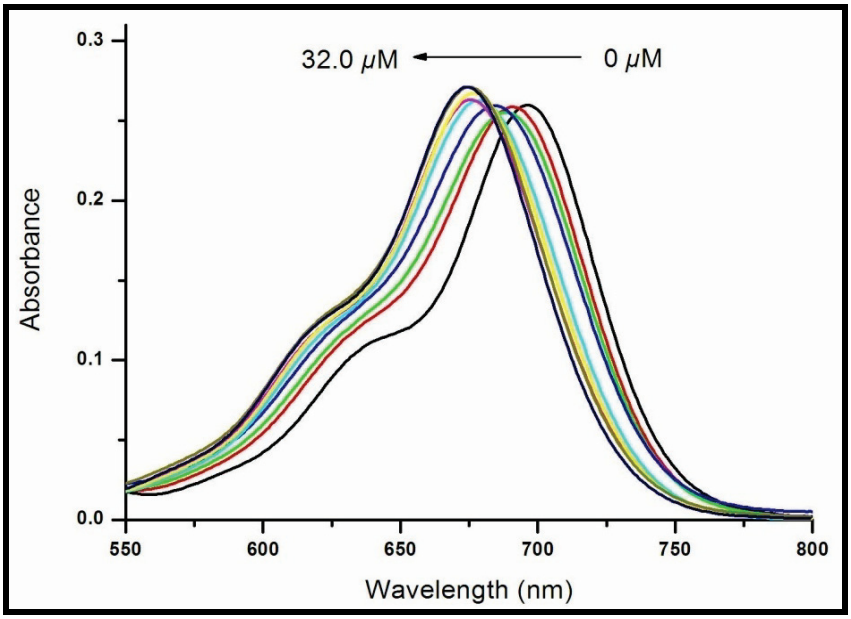

Figure 42. Absorbance spectra of compound **4** in acetonitrile in the presence of increasing Zn(II) concentrations (0, 3.2, 6.4, 9.6, 12.8, 16.0, 19.2, 25.6, 32.0 μM).

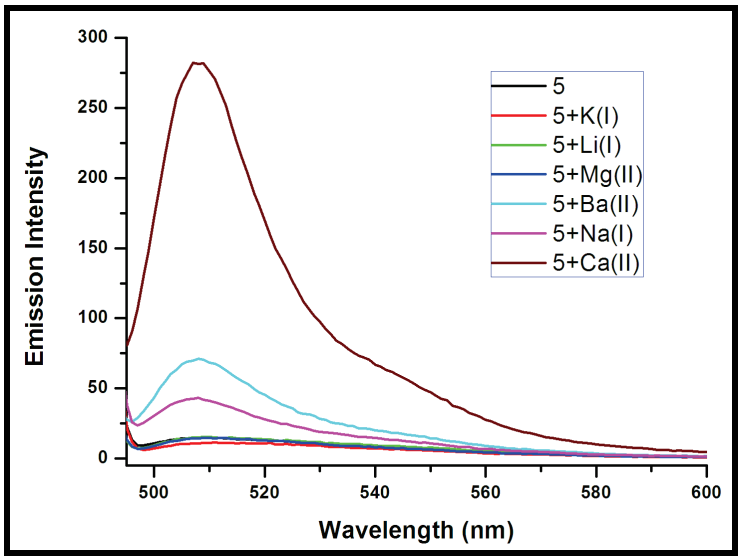

Figure 43. Emission spectra of compound 5 (1.67 μM) in acetonitrile in the presence of various cations (cation concentrations are 1.67 mM). (λ_{ex}=495 nm)

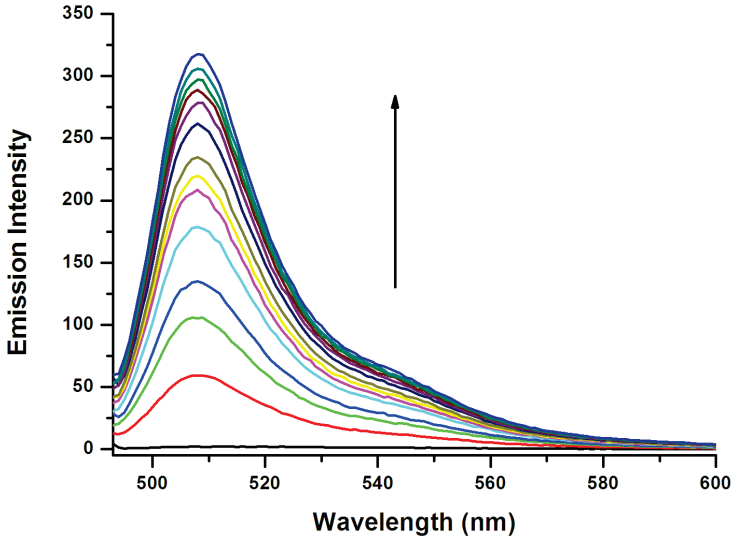

Figure 44. Emission specta of compound **5** (1.67 μM) in acetonitrile in the presence of increasing Ca(II) concentrations (0.0, 0.17, 0.33 0.5, 0.67, 0.83, 1.0, 1.17, 1.33, 1.5, 1.67, 1.83, 2.0, 2.17 mM).

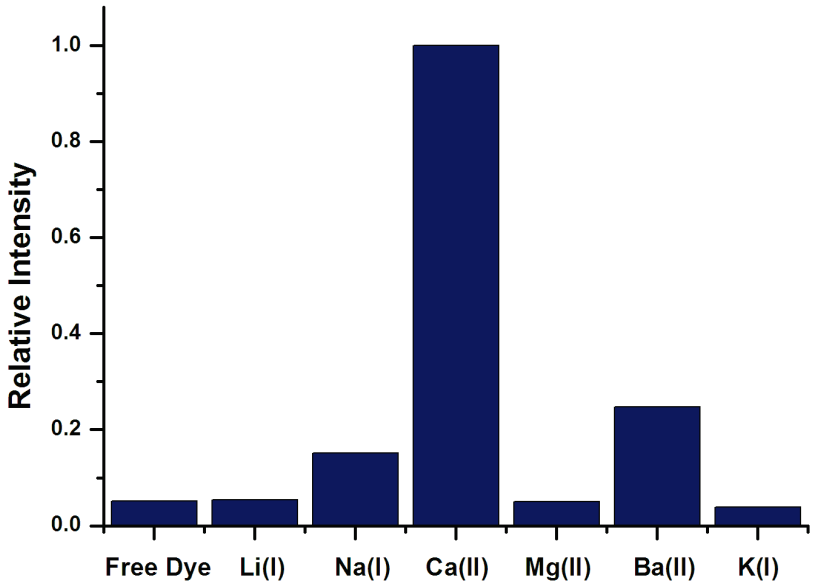

Figure 45. Emission ratios for compound **5** obtained in the presence of different cations. Samples were excited at 495 nm and the normalized emission intensity values at 510 nm are shown on the y-axis.

APPENDIX B

ADDITIONAL ITC DATA

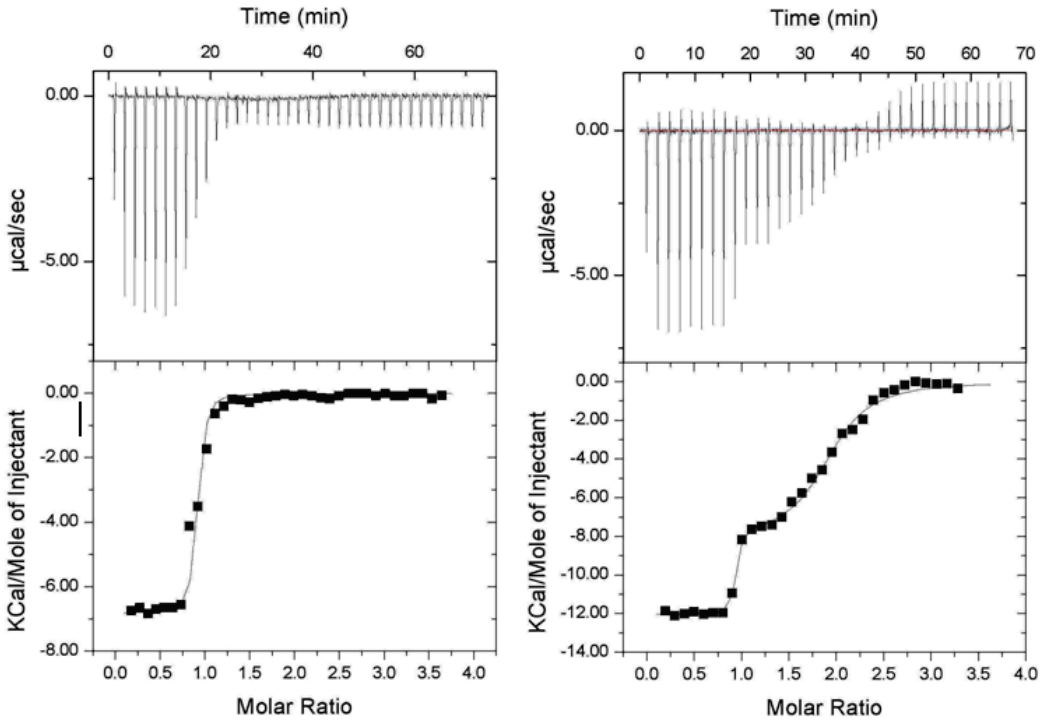

Figure 46. ITC titration curves of compound **2** in acetonitrile. Left: 0.3 mM **2** titrated with 5.5 mM $Zn(ClO_4)_2$, Right: b) 0.3 mM **2** titrated with 5mM $Hg(ClO_4)_2$.

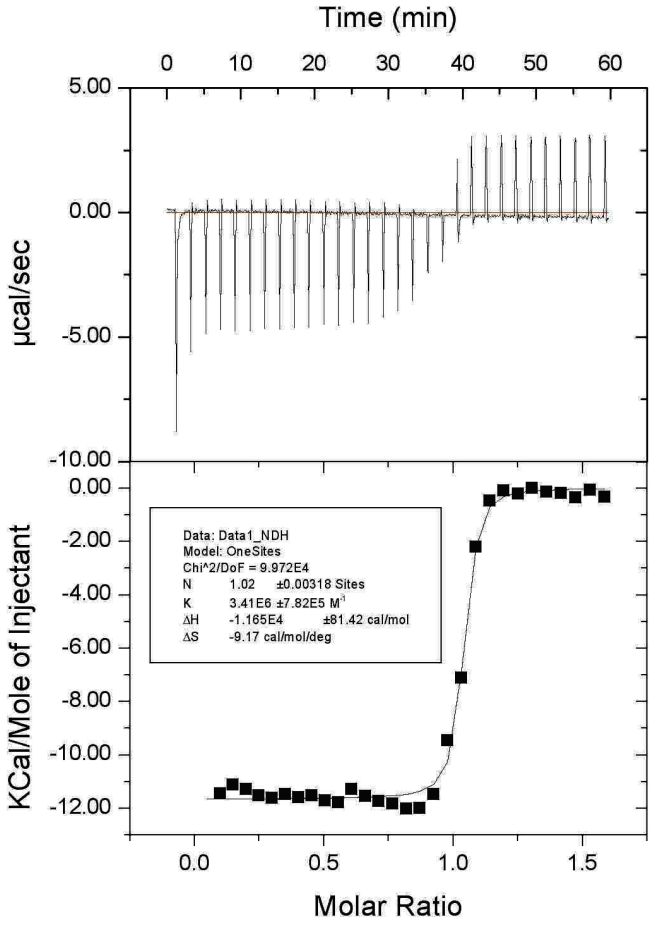

Figure 47. ITC titration curve of a reference compound N-(4-formylphenyl)-aza-4,13-dithia-[15]crown-5. 0.5 mM solution of the ligand was titrated with 5.0 mM $Hg(ClO_4)_2$.

APPENDIX C

NMR SPECTRA

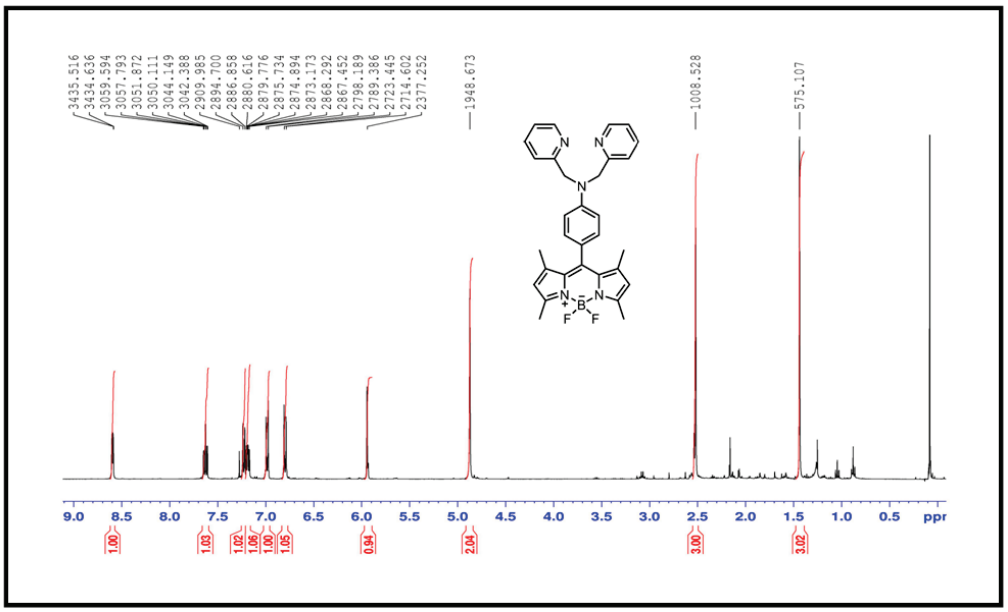

Figure 48. ^{1}H NMR spectrum of **1** (400 MHz, $CDCl_3$)

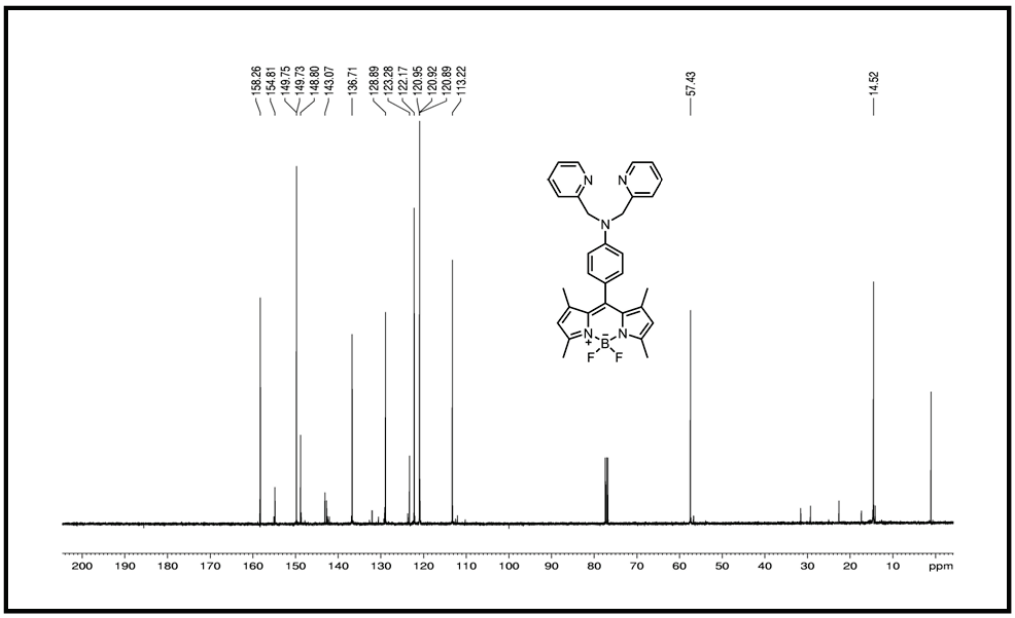

Figure 49. ^{13}C NMR spectrum of **1** (100 MHz, $CDCl_3$).

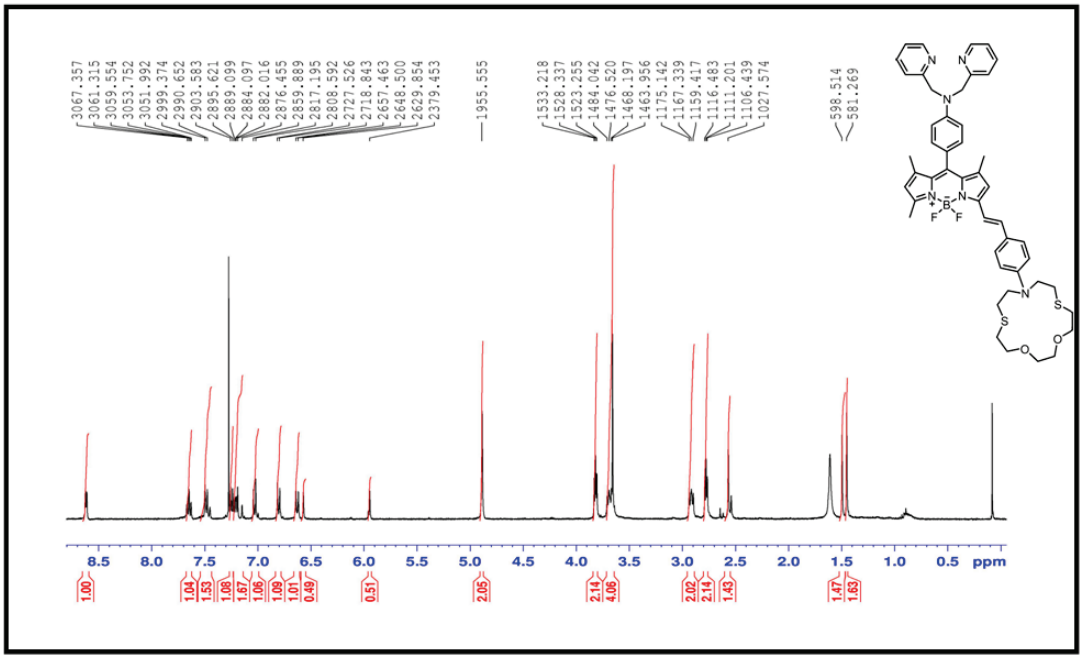

Figure 50. ^{1}H NMR spectrum of **2** (400 MHz, $CDCl_3$).

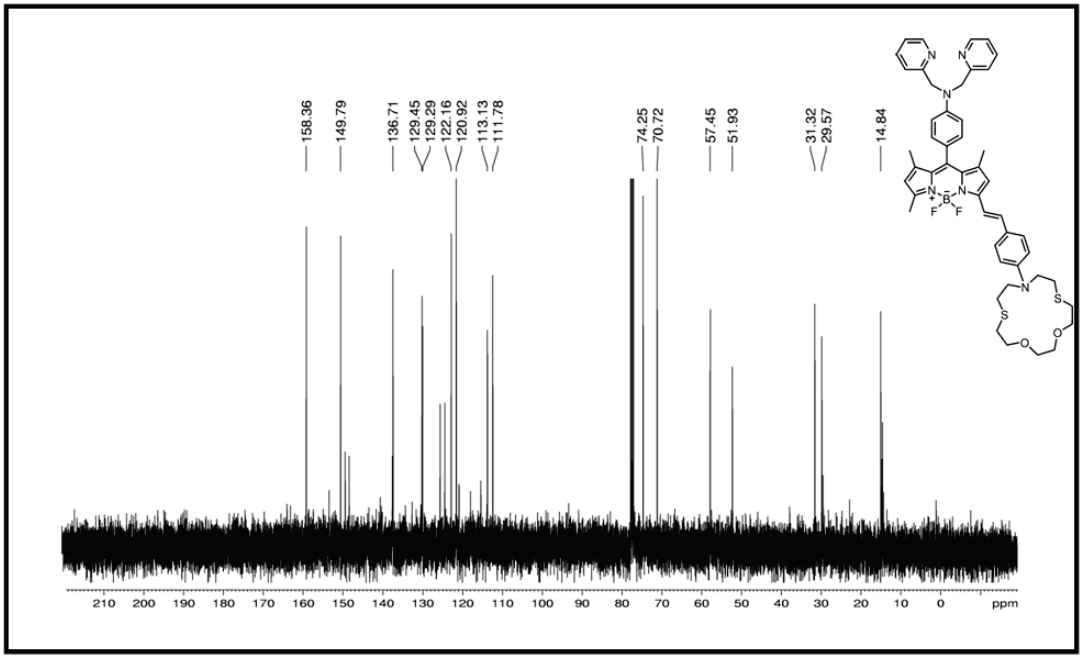

Figure 51. ^{13}C NMR spectrum of **2** (100 MHz, $CDCl_3$)

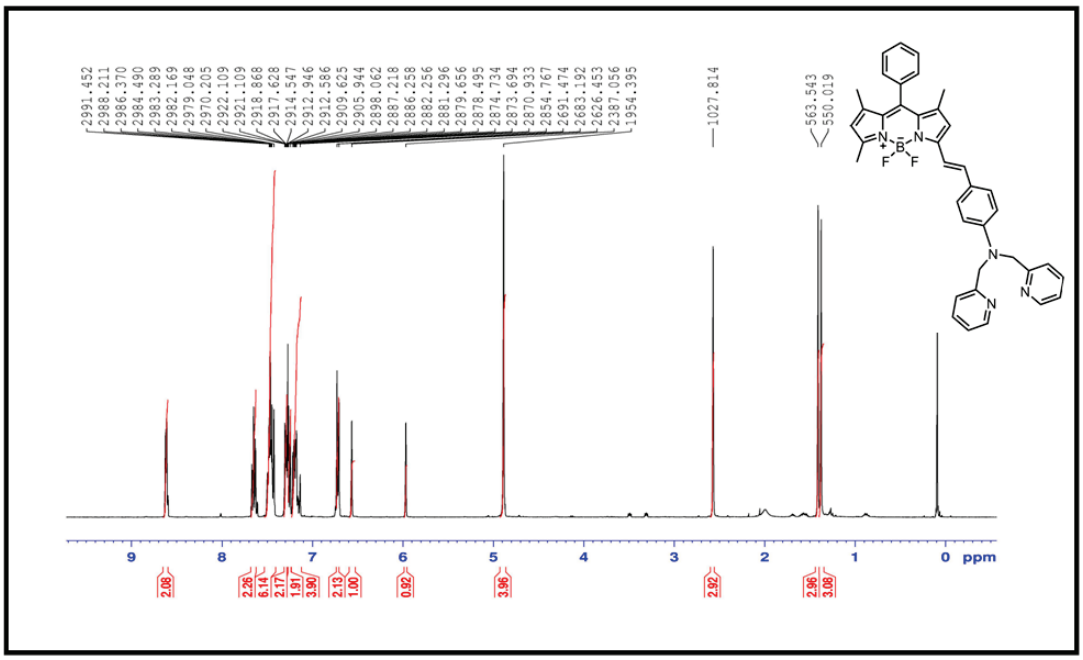

Figure 52. ^{1}H NMR spectrum of **3** (400 MHz, $CDCl_3$)

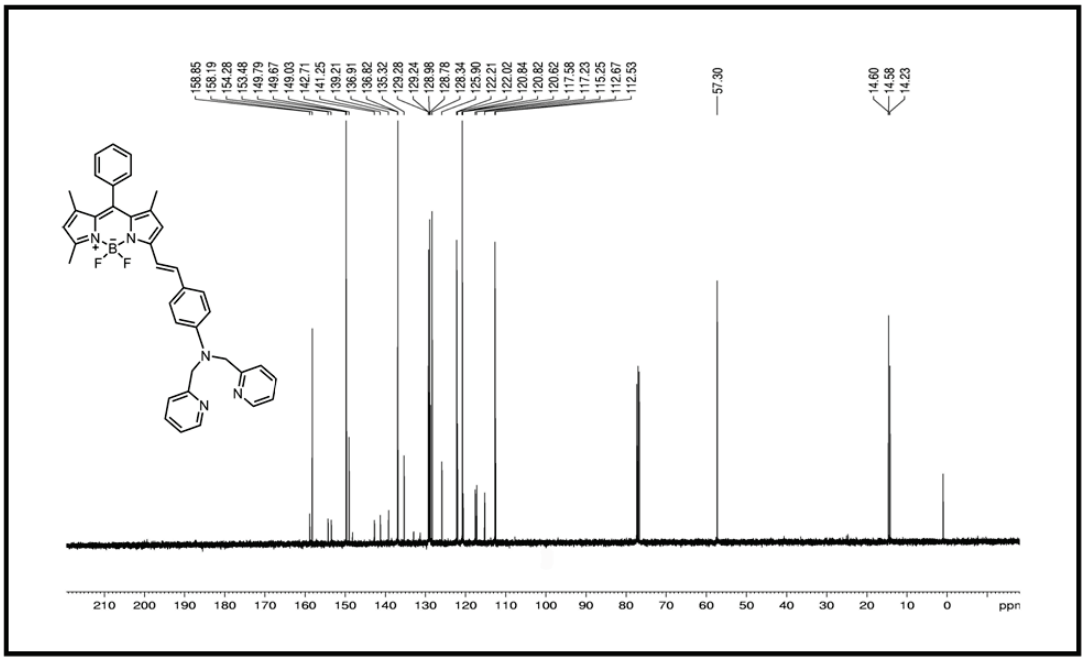

Figure 53. ^{13}C NMR spectrum of **3** (100 MHz, $CDCl_3$)

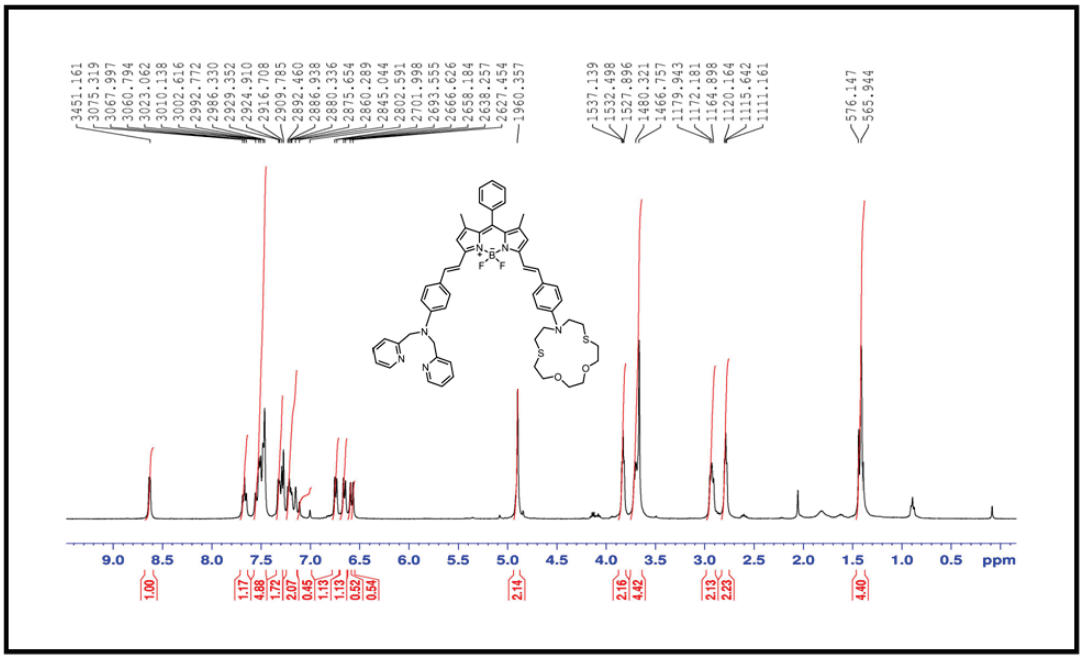

Figure 54. ^{1}H NMR spectrum of **4** (400 MHz, $CDCl_3$)

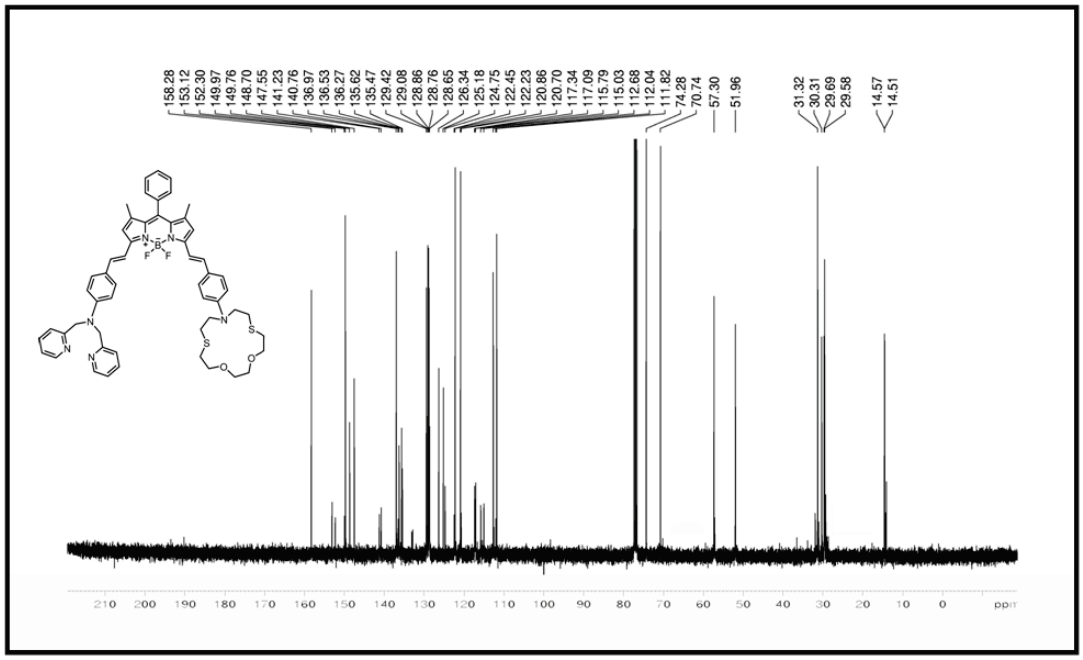

Figure 55. ^{13}C NMR spectrum of **4** (100 MHz, $CDCl_3$)

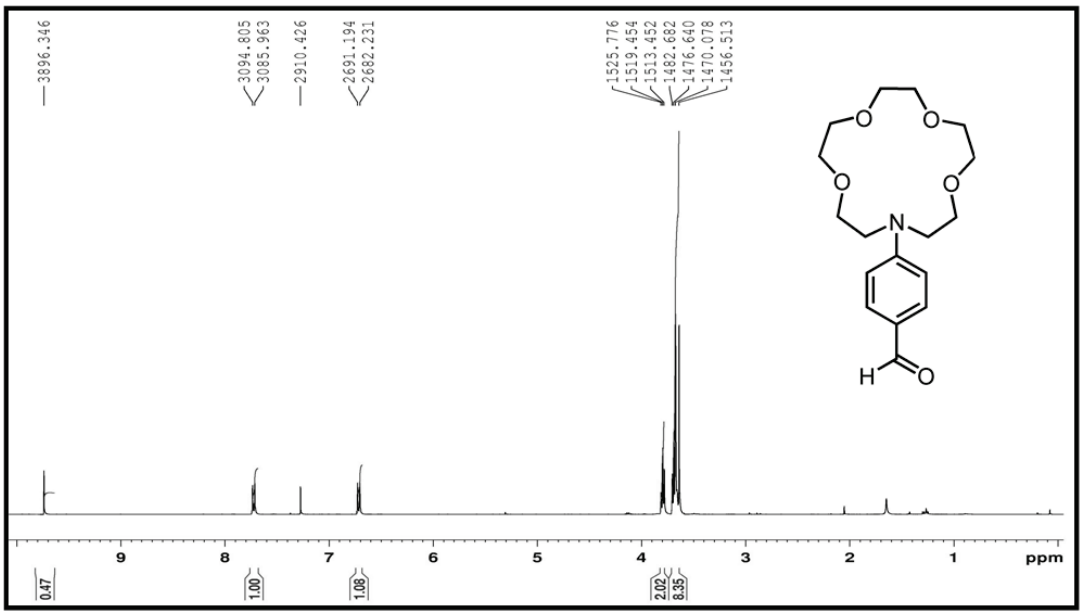

Figure 56. ^{1}H NMR spectrum of N-(4-formylphenyl)-1-aza-4,13-dithia-15-crown-5 (400 MHz, $CDCl_3$)

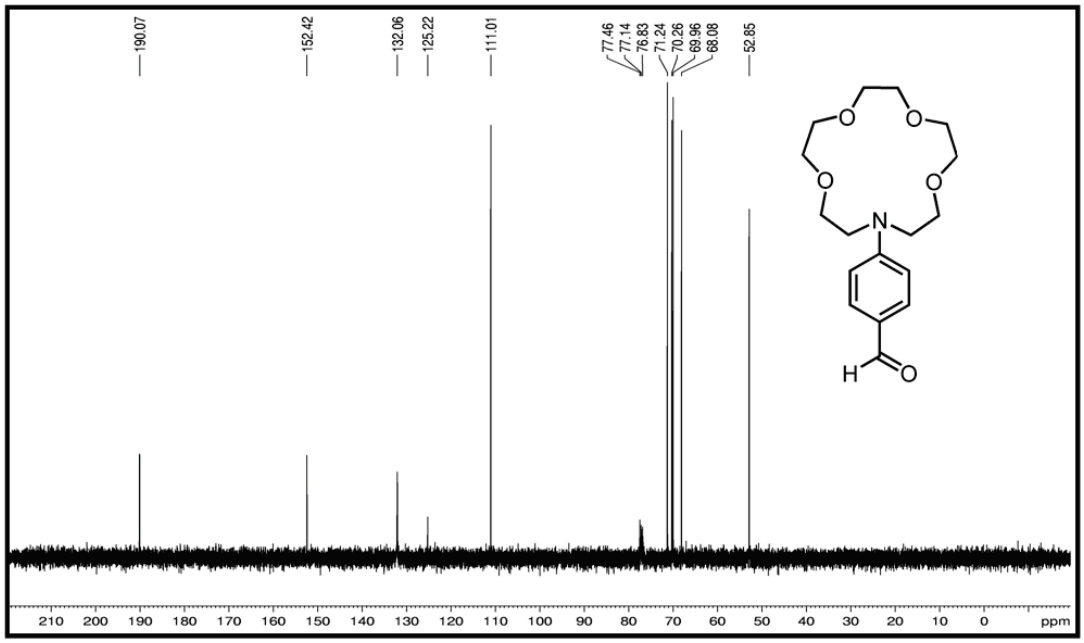

Figure 57. ^{13} C NMR spectrum of N-(4-formylphenyl)-1-aza-4,13-dithia-15-crown-5 (100 MHz, $CDCl_3$)

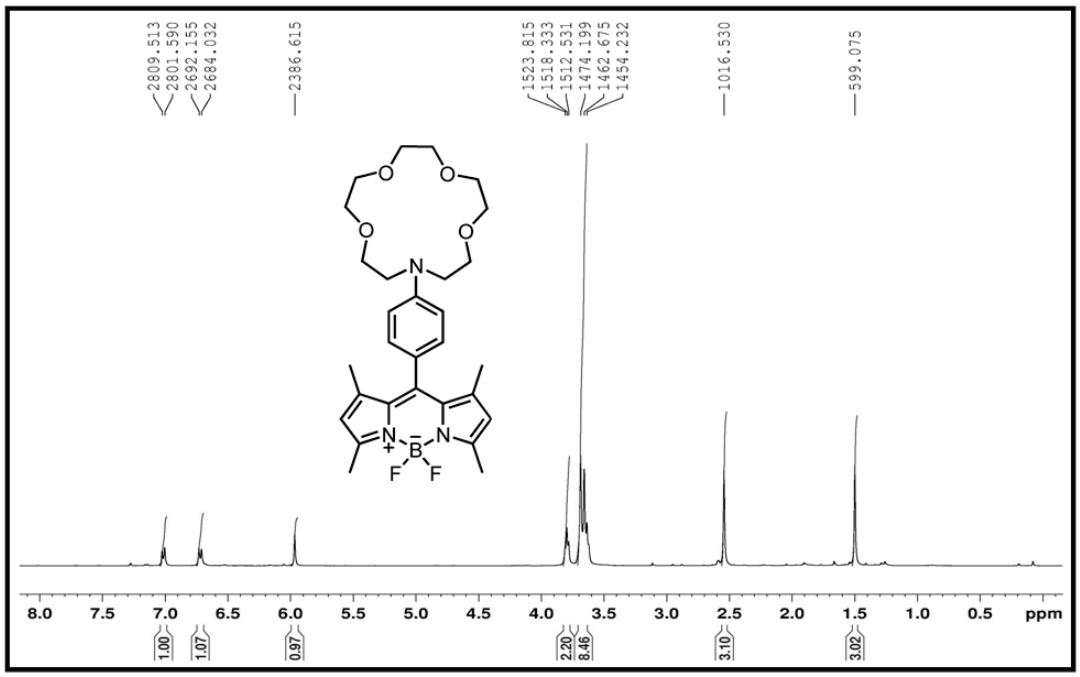

Figure 58. 1H NMR spectrum of **4** (400 MHz, CDCl3)

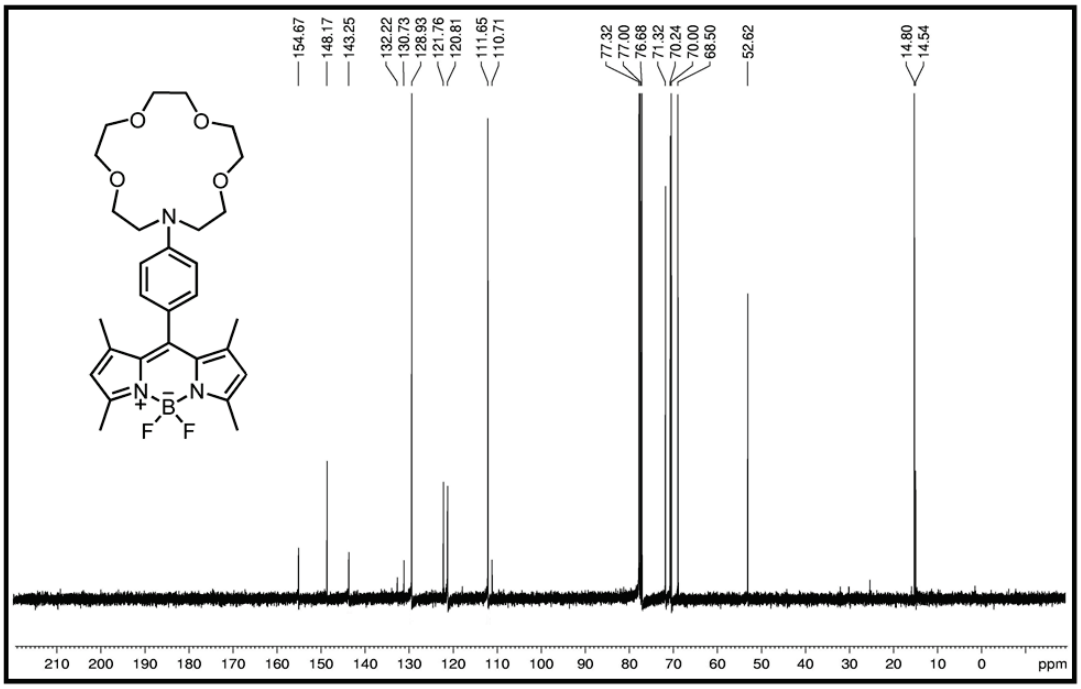

Figure 59. ^{13}C NMR spectrum of **5** (100 MHz, $CDCl_3$).

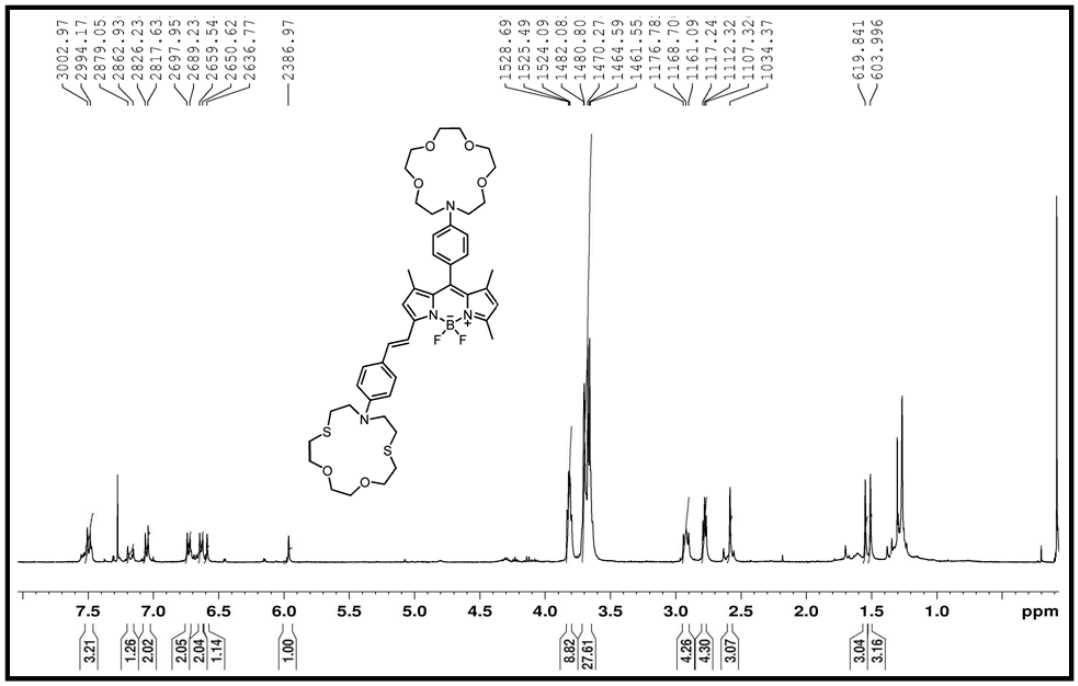

Figure 60. ^{1}H NMR spectrum of **6** (400 MHz, $CDCl_3$)

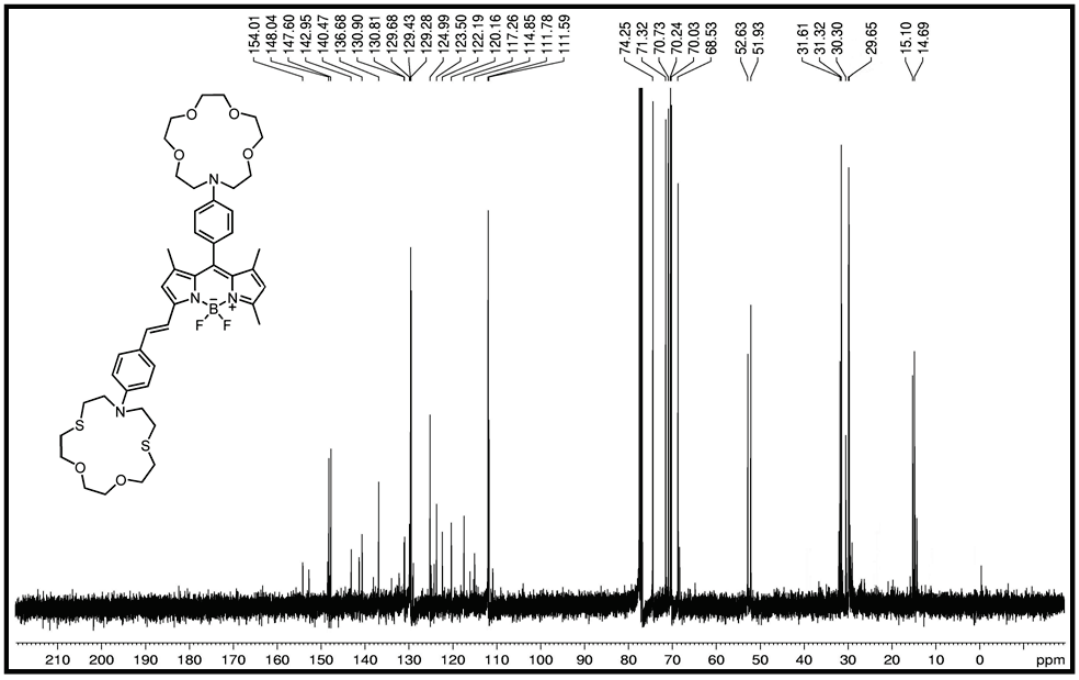

Figure 61. ^{13}C NMR spectrum of **6** (100 MHz, $CDCl_3$)

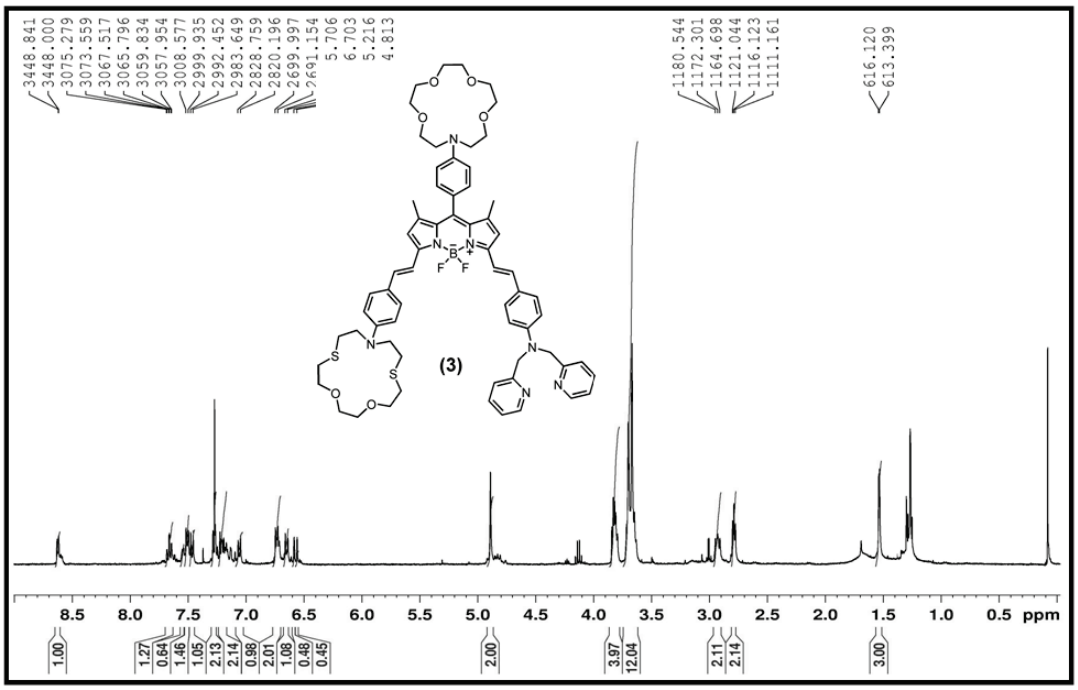

Figure 62. ^{1}H NMR spectrum of **7** (400 MHz, $CDCl_3$)

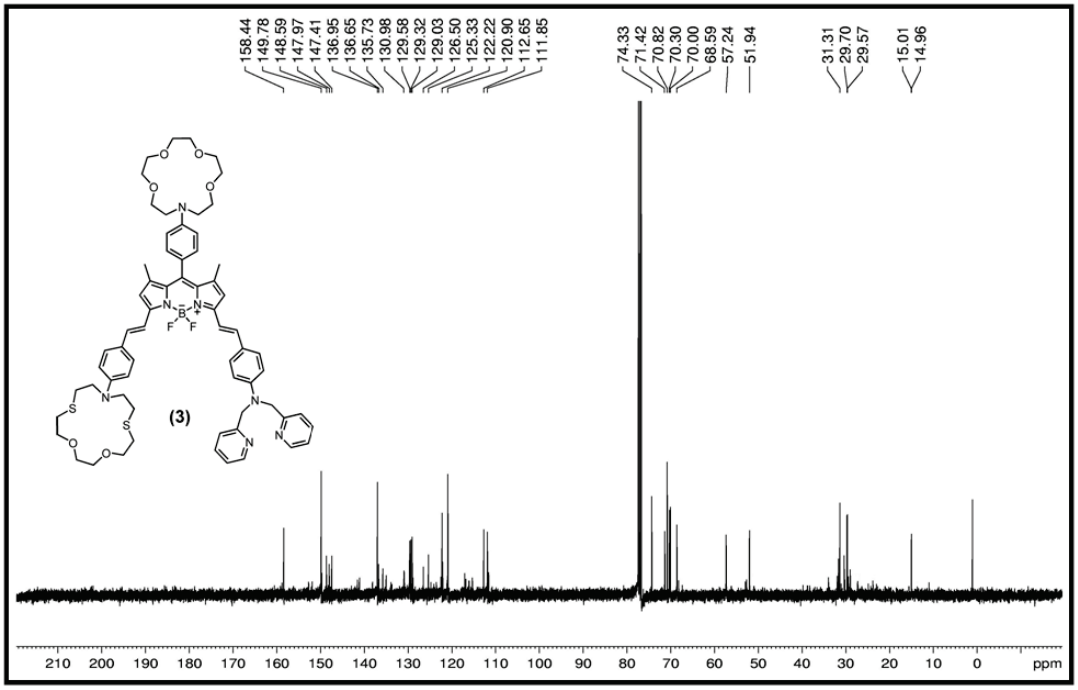

Figure 63. ^{13}C NMR spectrum of **7** (100 MHz, $CDCl_3$).

APPENDIX D

MASS SPECTRA

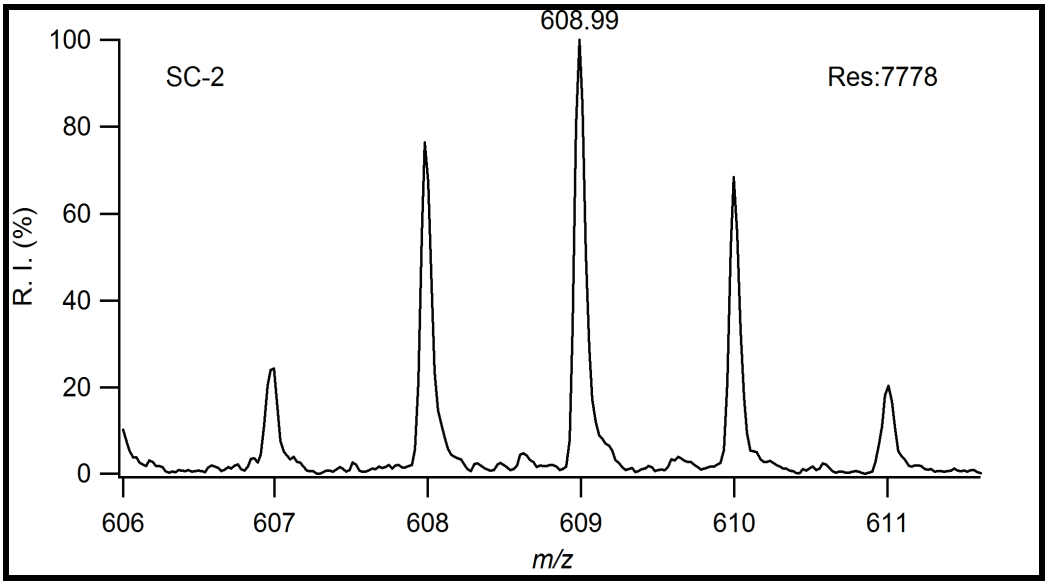

Figure 64. MALDI-TOF Mass spectrum of **2**

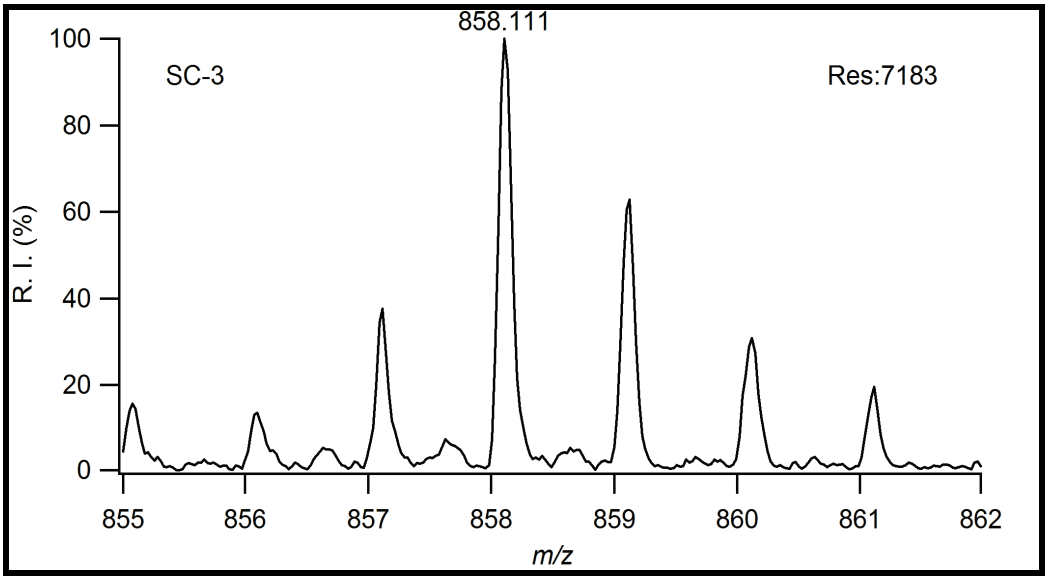

Figure 65. MALDI-TOF Mass spectrum of **3**

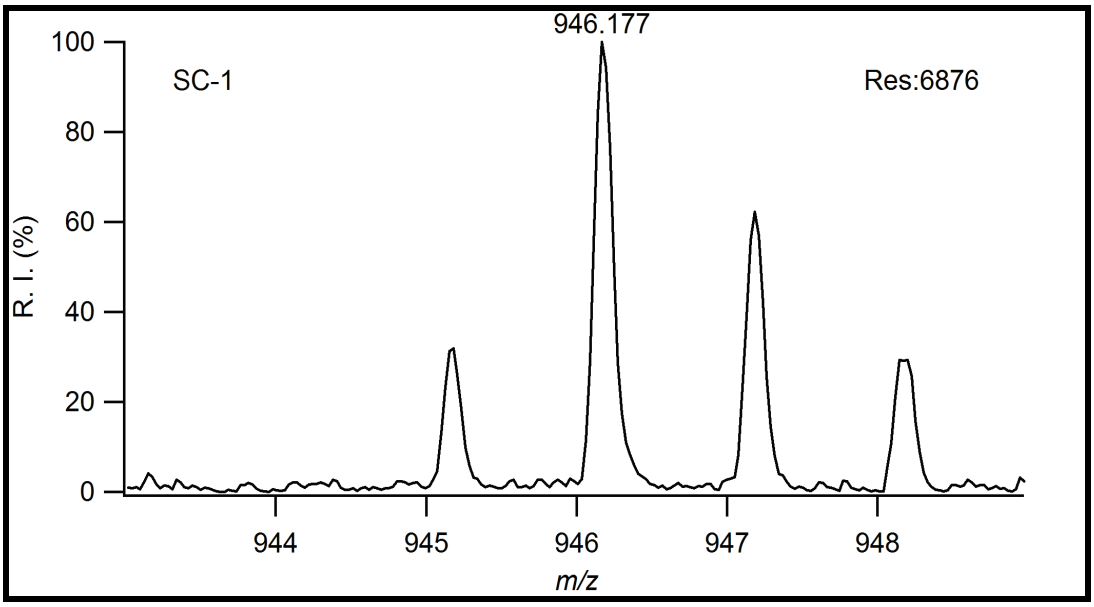

Figure 66. MALDI-TOF Mass spectrum of **4**

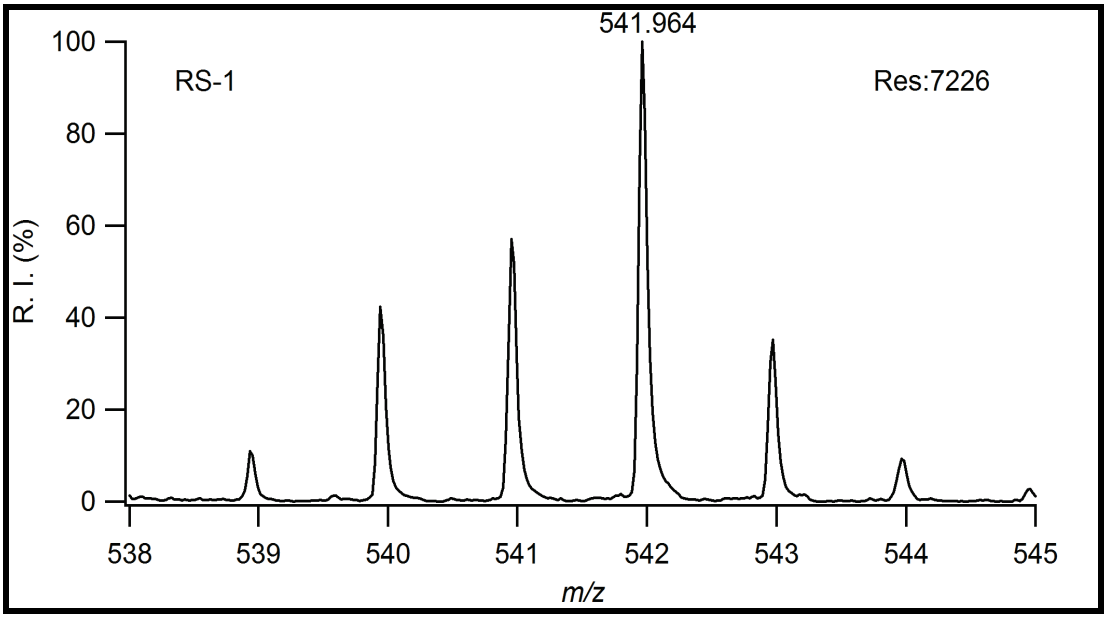

Figure 67. MALDI-TOF Mass spectrum of **5**

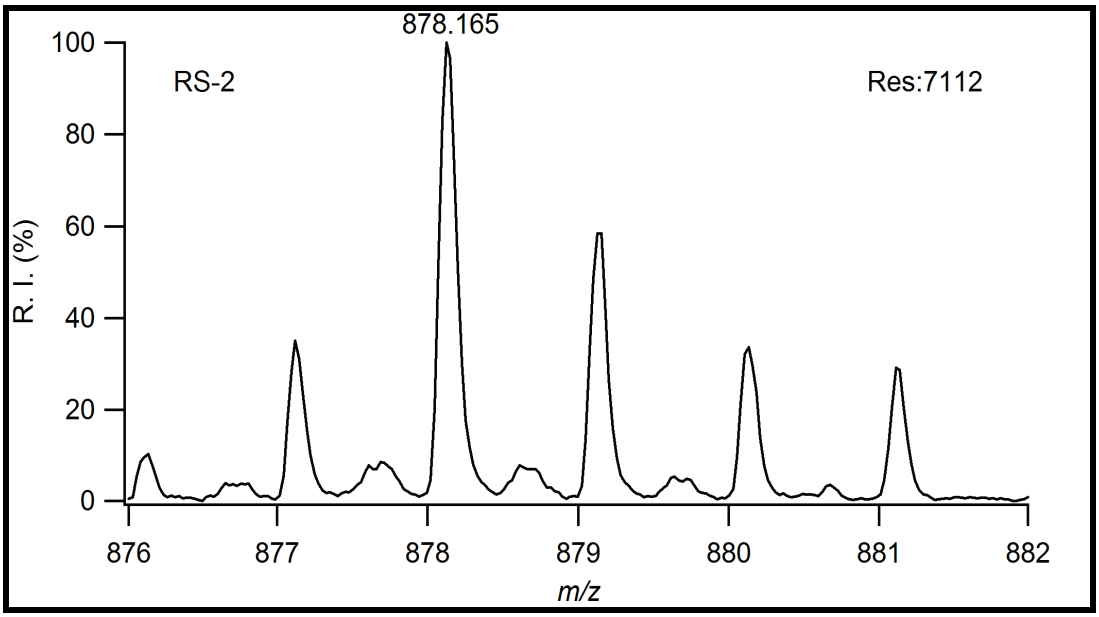

Figure 68. MALDI-TOF Mass spectrum of **6**

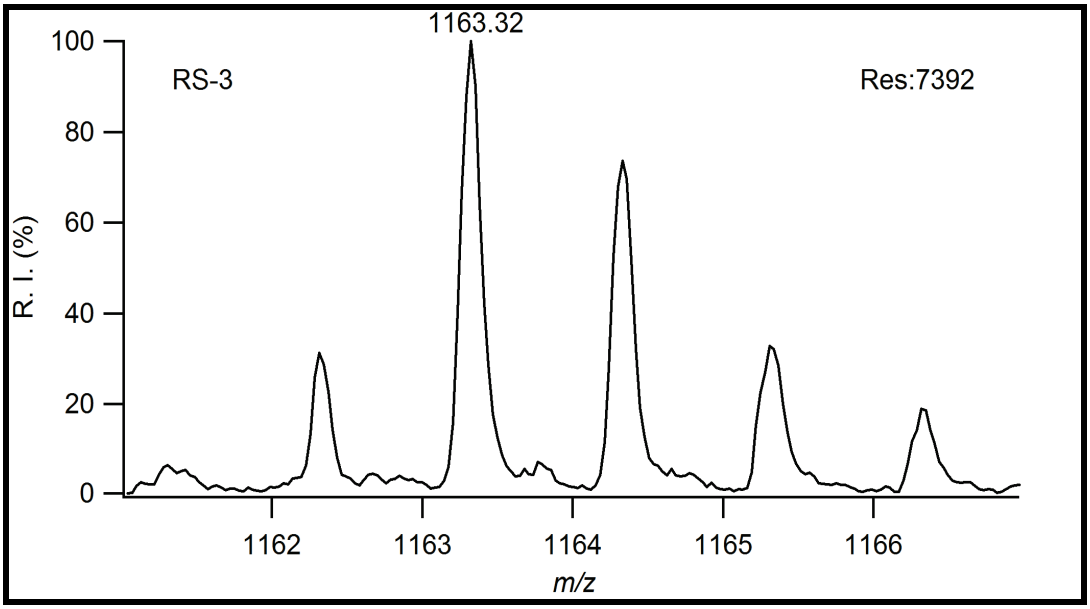

Figure 69. MALDI-TOF Mass spectrum of **7**